NUREG/CR-1948
EGG-2082
Distribution Category: R2

UO_2 DENSIFICATION IN LOFT FUEL

Charles S. Olsen

Published March 1981

EG&G Idaho, Inc.
Idaho Falls, Idaho 83415

Prepared for the
U.S. Nuclear Regulatory Commission
Washington, D.C. 20555
Under DOE Contract No. DE-AC07-76IDO1570
FIN No. A6053

ABSTRACT

The propensity of Loss-of-Fluid Test (LOFT) fuel pellets to densify was determined, and the effects of UO_2 densification on thermal and mechanical fuel rod behavior during a loss-of-coolant experiment were evaluated. The literature on UO_2 densification was reviewed to ascertain the important in-pile densification parameters, appropriate out-of-pile resintering tests for estimating the maximum in-pile densification, and the densification dependency on burnup. Maximum in-pile densification was estimated to be 3.5% theoretical density from out-of-pile resintering tests at 1973 K for 24 h. This densification may increase stored energy by 19.8 and 12.2% at reactor power levels of 26.3 and 52 kW/m, respectively. Densification is not expected to affect the fuel rod cladding; however, some buckling of the cladding may occur if compensating effects of pellet cracking and relocation or cladding creepdown do not occur.

SUMMARY

The propensity of Loss-of-Fluid Test (LOFT) fuel pellets to densify was determined, and the effects of UO_2 densification on thermal and mechanical fuel rod behavior during a loss-of-coolant experiment (LOCE) were evaluated. The literature on UO_2 densification was reviewed to ascertain the important densification parameters, appropriate out-of-pile resintering tests for estimating the maximum in-pile densification, and the densification dependency on burnup. The maximum in-pile densification was estimated from out-of-pile resintering tests at two resintering times and was characterized by immersion densities, length, diameter, and pore size distributions. The effects of densification upon stored energy and fuel rod cladding deformation were evaluated.

The resintering test procedure consisted of resintering UO_2 pellets from Lots 20-3 and 20-5 which are used in the first LOFT center fuel bundle. The pellets were resintered at 1973 K for 14 and 24 h to achieve the maximum densification. Pellets from Lot 20-3 densified to 3.16% theoretical density (TD) after resintering for 14 h. An additional 10 h at 1973 K resulted in an additional densification of 0.33% TD. However, pellets from Lot 20-5 densified to 3.68% TD after 14 h, but an additional 10 h produced pellet swelling of 0.28% TD so that the final densification decreased to 3.40% TD. This latter result may be attributed to pore coalescense when the pore pressure is in equilibrium with the surface tension. The change in pellet dimensions was anisotropic with a ratio of change in pellet length to change in pellet diameter between 1.15 and 1.19. Densification calculated from pore size distributions correlated well with the resintering results.

The rate of densification with burnup was calculated from a model derived using data from the Halden Test Reactor and the Electric Power Research Institute. This model predicts that the maximum densification in LOFT will be achieved within 1100 MWd/MtU. Based on FRAP-T5 computations, this maximum densification could cause an increase in stored energy of 19.8 and 12.2% at reactor power levels of 26.3 and 52 kW/m, respectively, considering only the changes in pellet dimensions.

ACKNOWLEDGMENTS

The author extends special thanks to M. W. Ellingford and P. B. Hembree for performing the resintering tests and the densification measurements and to G. L. Fletcher for the metallography and pore size measurements. The assistance of D. V. Miley for the scanning electron microscope photographs, W. E. Driskell for the FRAP computer code calculations, and R. R. Hobbins and E. L. Tolman for technical assistance is gratefully acknowledged.

CONTENTS

FIGURES

TABLES

UO_2 DENSIFICATION IN LOFT FUEL

INTRODUCTION

Irradiation-induced densification of sintered UO_2 pellet fuel results in fuel column shortening, the formation of axial gaps in the pellet fuel stack, and a postulated increase in fuel-cladding diametrical gap.[1] Fuel stack shortening and formation of axial gaps in the fuel pellet stack may affect the extent of cladding deformation (waisting) in unpressurized fuel rods during a loss-of-coolant transient.[2] If an increase in diametrical gap occurs during steady-state operation, an accompanying increase in volumetric power generation may lead to higher fuel temperatures and a corresponding increase in stored energy and possible fission gas release, compared with stable fuel.

This report presents results of a study to determine the propensity of sintered UO_2 fuel pellets to densify during operations in the Loss-of-Fluid Test (LOFT) facility. The results of the study will be used (a) to calculate the stored energy of the fuel and cladding deformation during LOFT loss-of-coolant experiments (LOCEs), and (b) to quantify differences in behavior compared with standard, light pressurized water reactor (LPWR) stable fuel pellets.

The LOFT facility is a 50-MW(t) pressurized water reactor (PWR) designed to simulate ~1000 MW(e) commercial PWR operations and thermal-hydraulic conditions during postulated accidents. The LOFT facility and experimental program are described in Reference 3. LOFT is sponsored by the U.S. Nuclear Regulatory Commission and is administered by the U.S. Department of Energy at the Idaho National Engineering Laboratory (INEL).

The LOFT fuel pellets are sintered UO_2 with 93% theoretical density. They are 9.27 mm in diameter and 15.2 mm long. The pellet stack length in the fuel rods is 1.68 m. The zircaloy-4 fuel rod cladding is 0.62 mm thick. The fuel rods are filled with helium. The fuel pellets used in this study were from Lots 20-3 and 20-5, the same as used in the first LOFT center fuel bundle.

The propensity of fuel pellets to densify can be determined from relatively simple out-of-pile resintering tests; however, the extent of densification must be related to actual in-pile densification. The pertinent densification literature is reviewed in this report to learn the nature of in-reactor densification and to select an out-of-pile procedure for measuring the propensity of LOFT fuel pellets to densify. The out-of-pile thermal densification tests performed with LOFT fuel and the pore size distribution for different heat treatments are described. A model based on the literature review and used to establish in-pile densification as a function of burnup for LOFT fuel is discussed. The potential effects of densification on the LOFT fuel rod behavior are also discussed. Following this discussion, the conclusions reached during the study are presented. The LOFT fuel pellet resintering procedure, Type C thermocouple calibration, and pore size characterization are described in Appendixes A, B, and C, respectively.

REVIEW OF DENSIFICATION PHENOMENON

In this section, results from prior investigations and models are studied in order to understand some parameters that can affect densification. In some cases, the conclusions reported by the various investigators are contradictory; therefore, a consensus of the results is presented.

Literature Review

Collins and Hargreaves[4] contrasted measurements of out-of-pile sintering rates of UO_2 fuel at temperatures greater than 1600 K with the sintering rates of fuel irradiated in the Windscale Advance Gas-Cooled Reactor (WAGR). The observed out-of-pile densification was attributed to the sintering of grain boundary porosity by grain boundary diffusion. Extrapolation of these results to the approximate 1000-K temperatures of the in-pile material indicated that negligible thermal sintering would be expected after a few hundred hours at this temperature. In addition, no evidence of sintering was observed in out-of-pile heating at 1173 K with a pressure of 2.06 MN/m^2 for several months. However, fuel irradiated to less than 0.3% burnup of heavy atoms at fuel surface temperatures between 1000 and 1100 K experienced significant reductions in the pellet diameters. The elimination of pores with diameters less than 3 μm was reported to be the major source of increased density. Pores larger than 100 μm were reported stable during irradiation at temperatures below 1500 K. The important densification parameters are burnup and initial porosity.

Collins and Hargreaves[4] suggested that a complete description of the densification rate of uranium dioxide under irradiation demands a knowledge of the initial size distribution of the as-manufactured porosity, in addition to the total volume of porosity, because of the differing sintering rates of pores of different sizes. However, the morphology of the porosity in the UO_2 fuel they used was not determined.

Rolstad et al.[5] measured the following characteristics during fuel rod irradiation in the Halden Heavy Boiling Water Reactor[a]: shortening of the UO_2 fuel stack with 87 to 95% theoretical density (TD), two different heat ratings, three different degrees of fuel stability as determined by the fuel sintering temperature, and two different gap widths. The axial length change was measured at time intervals during the irradiation of the rods.

The axial length change as a function of burnup for different power levels indicated very little difference in the densification of similar fuel rods operating at quite different power levels. This result suggests that in-pile fuel densification is probably independent of fuel temperature. This conclusion is in agreement with the fission-induced sintering rates proposed by Collins and Hargreaves.[4] However, Hanevick et al.[6] proposed that this may be attributed to the outer edges (shoulder) of the pellet being within 200 to 300 K of each other at both power levels. The amount of fuel stack shortening was found to depend mainly on the out-of-pile thermal fuel stability (sintering temperature), initial density, and burnup.

Rolstad et al.[5] used two equations to correlate their data. Using their first equation, Equation (1), the magnitude of shortening was calculated as a function of the percent theoretical density (DENS) and sintering temperature in Kelvin (TSINT) at a burnup of 5000 $MWd/MtUO_2$:

$$\left(\frac{\Delta L}{L}\right)_{max} = 22.2 \frac{(100 - DENS)}{(TSINT - 1453)} \qquad (1)$$

where $(\Delta L/L)_{max}$ is the maximum percent of change in radial dimensions.

The effect of burnup was introduced through the use of a master curve [see Equation (2)] created by shifting all curves vertically to agreement at 5000 $MWd/MtUO_2$ and then horizontally to achieve the best agreement at the low burnup portion of the curves:

$$\frac{\Delta L}{L} = \left(\frac{\Delta L}{L}\right)_{max} - 0.93\, e^{-BU} - 2.07\, e^{-35BU} \qquad (2)$$

where BU is the burnup ($MWd/kgUO_2$).

a. The reactor located in Halden, Norway.

Equation (2) gives a very rapid length change at low burnup and a much slower length change at higher burnup levels. After a burnup of 5000 to 6000 MWd/MtUO_2, very little additional densification was calculated. Figure 1[5] compares the results from this model with those from the Halden data.

Ferrari et al.[7] measured UO_2 fuel pellet densification using movable in-core flux detectors in commercial reactors and postirradiation examination of selected Saxton[a] test rods. Fuel densification was reported to occur quite rapidly initially, but to end, that is, become equal to the swelling rate, after 6000 to 10 000 MWd/MtU as shown by Figure 2. These results are consistent with the measurements of Rolstad et al.[5] The extent of densification for 92% TD fuel was reported to vary significantly with microstructure, but no details of the microstructure were reported.

Ferrari et al.[7] reported that power levels between 4.9 and 55.8 kW/m did not significantly affect densification. This result is also in agreement with Collins and Hargreaves[4] and Rolstad et al.[5] The axial shrinkage was suggested to be controlled by densification in the shoulder of the fuel pellets, a region of the fuel pellets that generally operates at temperatures below 1073 K. These temperatures are too low for in-pile densification to be accounted for by thermal mechanisms, and Ferrari et al. proposed that the kinetics of densification are compatible with irradiation-enhanced diffusion processes.

Metallographic measurements on the Saxton fuel indicated that the irradiation-enhanced densification was associated with the disappearance of fine pores, and pore shrinkage significantly decreased with increasing pore size. However, in some fuels not all fine porosity disappears during irradiation because of increased pressure from entrapped gas. Ferrari et al. suggested that densification could be reduced through both microstructural control of the fuel pellet and a reduction of the fine porosity content. Both of these factors are influenced by the pellet fabrication process, especially sintering temperature and the use of so called "pore formers." Ferrari et al. reported that experimental fuel of 89% TD has been made and demonstrated in the Saxton reactor to be relatively stable.

Heal et al.[8] have developed stable-density UO_2 fuel through control of porosity size. They calculated that shrinkage of closed pores would continue until the internal pressure of trapped gas in the pores matched the surface tension forces causing shrinkage.

Fuel pellets with a 91 to 95% TD and porosity sizes greater than 25 μm manufactured by the controlled-porosity method were irradiated by Heal et al.[8] to 1.4×10^{26} fissions/cm^3 with center temperatures up to 1873 K. Postirradiation examination of these pellets showed significantly less than 1% volume densification.

Burton and Reynolds[9] measured the shrinkage of UO_2 fuel pellets of 96.5% TD during the final stage of out-of-pile sintering with isolated porosity located at grain boundaries. The density change as a function of time was measured for three specimens at different temperatures. The densification rate initially occurred very rapidly and then decreased to a much slower rate at longer times. The shapes of these curves are very similar to those for the in-pile densification of UO_2; however, in-pile densification apparently occurs at much lower temperatures. This reduction in the sintering rate with time can arise for several reasons: (a) grain boundaries may migrate away from cavities during annealing, thus removing the short-circuiting diffusion path of vacancies away from cavities; (b) when significant entrapped gas is present, cavities may shrink until they become stabilized as the internal gas pressure becomes equal to the surface tension of the cavity as proposed by Heal et al.[8]; or (c) the number of cavities can progressively reduce as densification proceeds. The first and second reasons were rejected by Burton and Reynolds because (a) the majority of the cavities in their samples remained on grain boundaries during sintering, and (b) smaller cavities closed during sintering. Therefore, Burton and Reynolds[9] suggest that the reduction in the sintering rate with time is due only to the progressive reduction in the number of cavities. In this case, the shape of the sintering curve is expected to be predicted quantitatively from the porosity distribution and a Hull and Rimmer[10] relationship. The decrease in sintering rate with time was found to be associated with only the progressive reduction in the number of

a. A small prototype, closed cycle PWR designed by the Westinghouse Electric Corporation and located in Saxton, Pennsylvania.

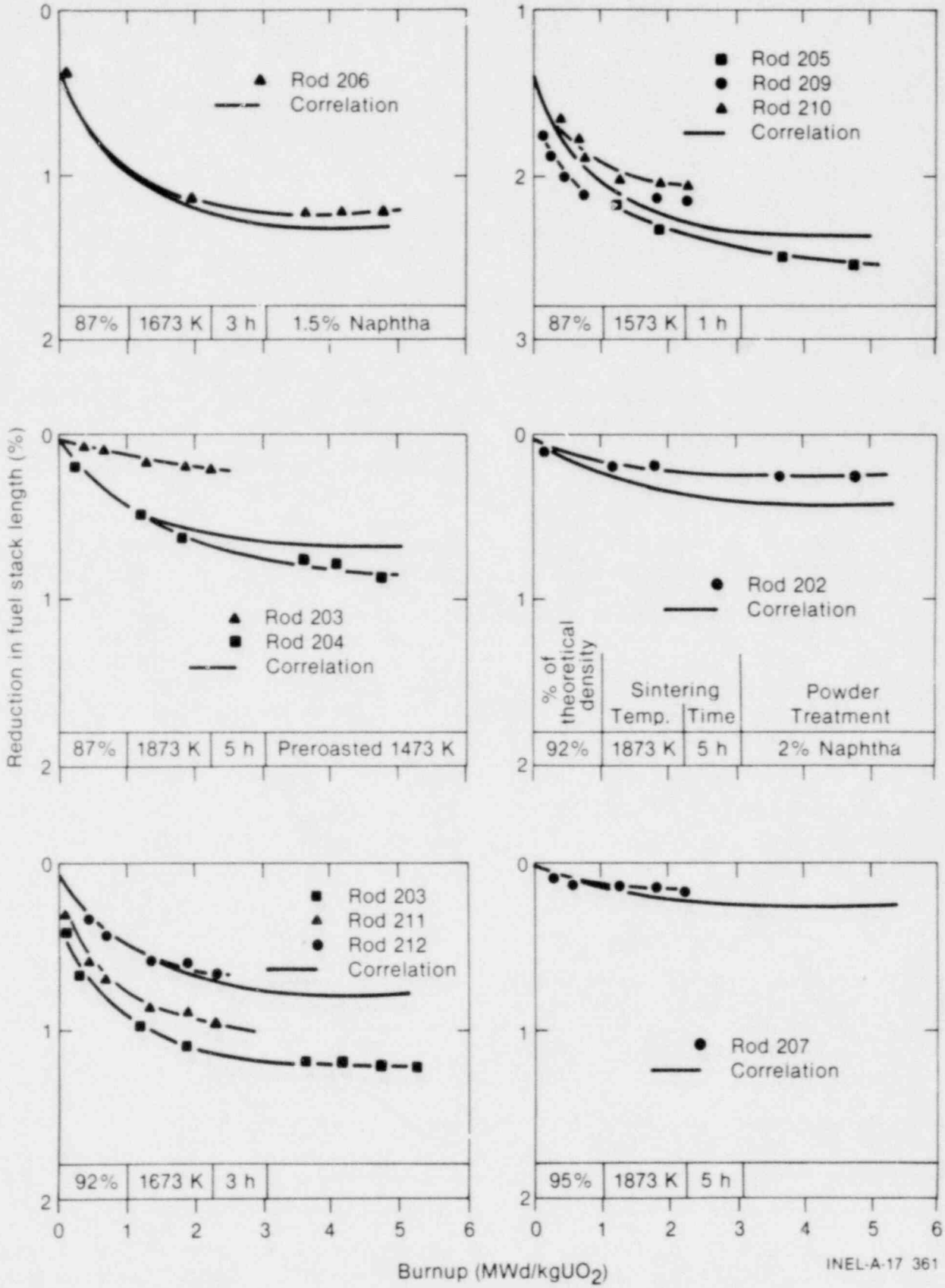

Figure 1. Comparison between measured and predicted fuel stack shortening.

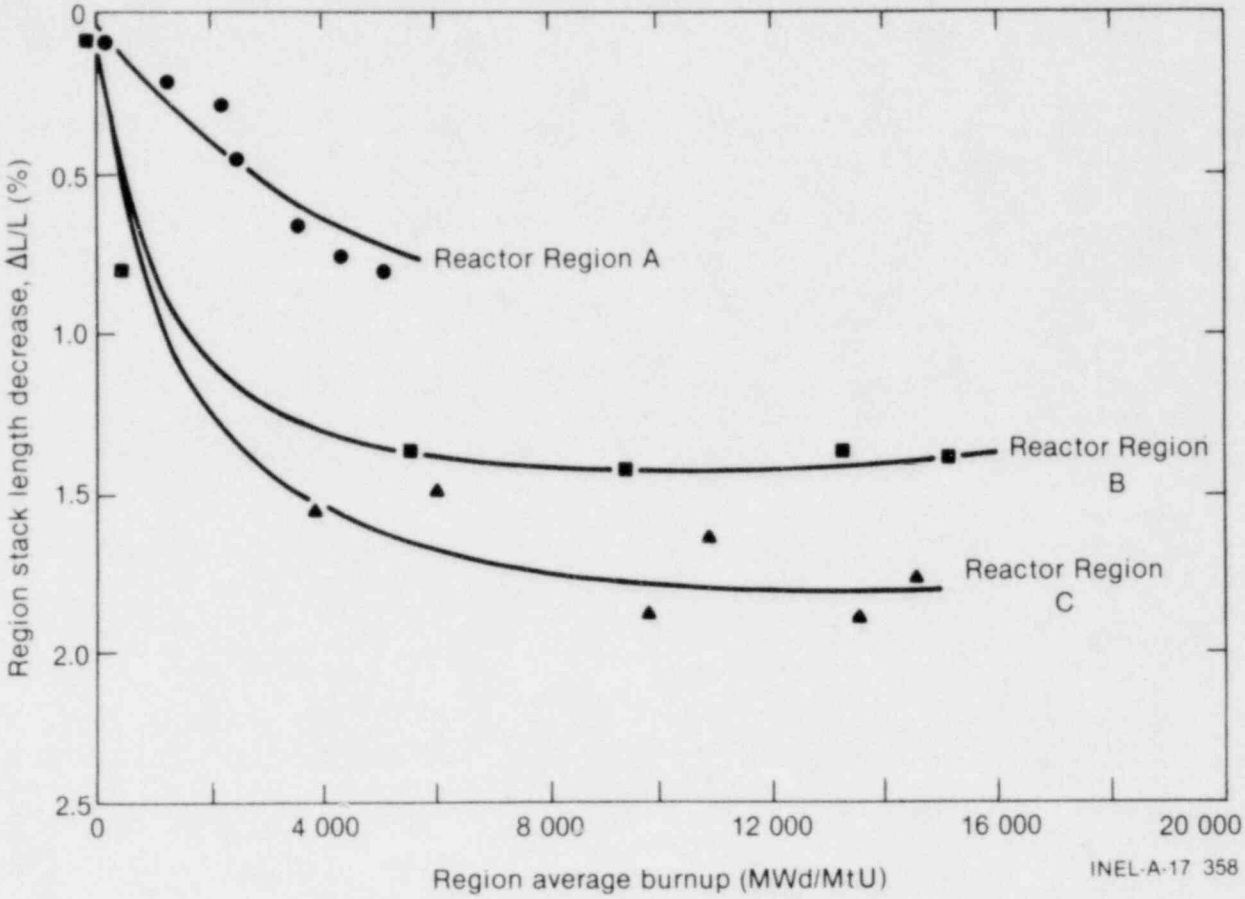

Figure 2. Fuel stack length changes for 92% TD UO_2 processed by different techniques.

cavities. However, the calculation was considered approximate because a constant cavity spacing was assumed for each time step in changing from one volume size to the next.

The similarity between the out-of-pile densification and in-reactor densification strongly suggests the importance of pore size distribution and volume to in-reactor densification.

Marlowe[11] proposed a model for diffusion-controlled densification and modified the model to include fuel swelling contributions to the density changes as well as an irradiation-induced diffusivity which provides atomic mobility for grain growth and densification.

The model is based on densification and grain growth rate parameters, which must be determined experimentally for any particular fuel. These parameters strongly affect the predicted in-reactor densification behavior through grain size modification. The model allows for complete pore elimination and, in fact, densities greater than theoretical for the matrix material. Thus, an upper limit to the density must be calculated.

The parameters used in this model (grain growth rate, grain size, and diffusion coefficient) strongly imply that material properties affect the extent of densification.

An extensive densification study was begun in 1973 by the Edison Electric Institute (EEI) and Electric Power Research Institute (EPRI) to investigate irradiation induced densification of UO_2 pellet fuel and relate densification behavior to pellet characteristics and irradiation conditions.[12,13] The results of this experimental program show that for the fuel types studied, the propensity for sintered UO_2 pelletized fuel to undergo irradiation induced densification can be correlated with fuel microstructure. The largest in-reactor density changes occurred for those types having a combination of the smallest pore size, the largest percent porosity less than 1 μm diameter, the smallest initial grain size, and the lowest initial density. Densification behavior cannot be defined

by any one of these parameters alone, but appears to be dependent on a combination of all these pellet characteristics. The volume fraction of porosity less than 1 μm in diameter contributed significantly to densification of the fuel types studied; density increases were accompanied by a significant decrease in the volume fraction of pores in this size range. The volume fraction of pores between 1 and 10 μm initially increased with densification, but with continued densification, the volume of these pores decreased.

In-pile densification was found to be dependent on fission rate, fuel temperature, and burnup (see Figure 3). For those fuel types that were prone to densify, densification occurred rapidly during irradiation at fission rates of 9.6 to 14.1 x 10^{12} fissions/cm^3•s and centerline temperatures of 1183 to 1600 K. Under these conditions, maximum density was approached at burnups as low as about 2 x 10^{19} fissions/cm^3 (~840 MWd/MtM).

The out-of-pile densification was correlated with in-pile densification. The density changes that occurred in out-of-reactor resintering tests at 1573 K for 1500 h, 1873 K for 48 h, and 1973 K for 14 h were all equivalent (within ±0.66% TD) to in-pile densification at a fission rate of 1.3 x 10^{13} fissions/cm^3•s for 1629 h (~3000 MWd/MtU).

The EPRI data in Figure 3 show that pellets located in low burnup, low fission rate regions densify about 67% less than pellets irradiated to the same burnup but in higher fission rate and temperature positions. At the higher fission rates and temperatures, densification occurs rapidly and

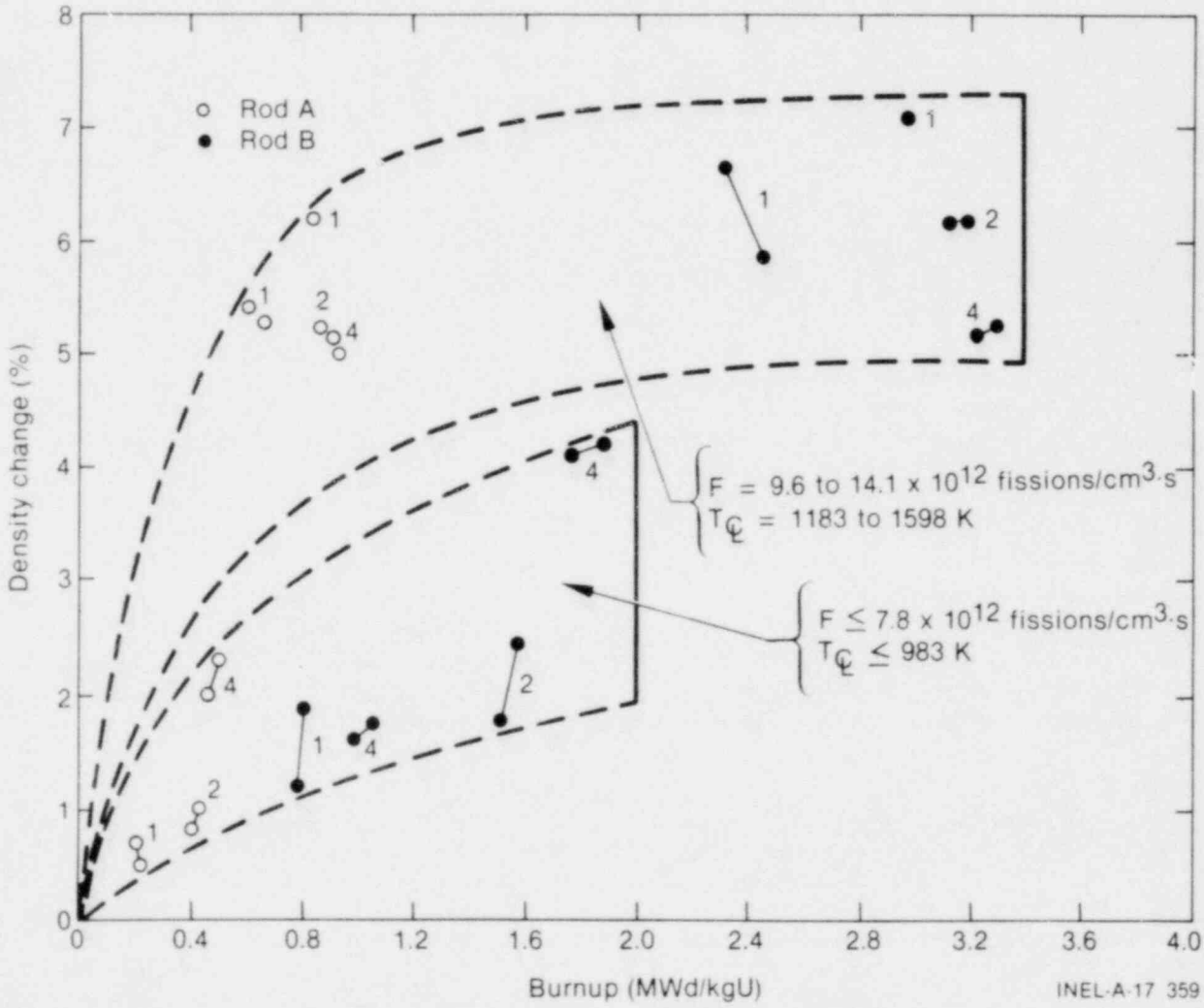

Figure 3. The effect of burnup and fission rate on the density change for EPRI fuel Types 1, 2, and 4.

pellets approach maximum densities at about 1 MWd/kgU. At lower fission rates, densification is not complete until about 2 MWd/kgU.

R. O. Meyer[14] developed a new model for the Nuclear Regulatory Commission (NRC) that was described as simple, conservative, and nonproprietary. Empirical correlations were included for the maximum density change and for densification kinetics. The model differentiates between stable (less than 4% TD densification) and unstable fuels (more than 4% TD densification) in the kinetics of densification. This 4% TD limit for stable fuels appears rather arbitrary, since it is based on only one data point of 7% TD.

The maximum density change is based on a 24-h, 1973-K resintering anneal. This anneal was selected because the resulting density change bounds most in-reactor density changes for a wide range of fuel types, and the final density is rather insensitive to exact annealing time for times greater than 24 h. Since the EEI/EPRI tests indicated a 14-h anneal was equivalent to about 3000 MWd/MtU, this resulting anneal of 24 h is equivalent to a burnup between 6000 and 10 000 MWd/MtU.

The burnup dependency is based on Halden data.[5] Best-fit lines to the density change versus logarithm of burnup resulted in an apparent zero Δo intercept of 20 MWd/MtU for stable fuels and 5 MWd/MtU for unstable fuels. A linear extrapolation from these intercepts to the maximum density change result in maximum densification occurring within 500 MWd/MtU for unstable fuels and 200 MWd/MtU for stable fuels. These values are conservative with respect to the Halden data. Additional conservation results by applying an upper one-sided 95/95 tolerance limit to the 24-h resintering density change to determine the maximum density change.

Consensus of Results

The general mechanics of fuel densification appear to be understood, although a model of the phenomena based on first principles is not available.

Collins and Hargreaves[4] suggested that in-reactor densification is radiation-induced; whereas, Ferrari et al.[7] proposed irradiation-enhanced thermal densification. However, both authors reported that their in-reactor densification was independent of temperature. Therefore, irradiation-induced densification appears to be the appropriate mechanism. The in-reactor densification rate was observed by Rolstad et al.[5] and Ferrari et al.[7] to decrease with burnup and to become zero near 5000 to 10 000 MWd/MtU. At this burnup, most of the fine porosity has disappeared, and the remaining porosity is beginning to fill with fission gases. Also, fuel swelling may compensate for densification at higher burnups. Empirical exponential equations were proposed by Collins and Hargreaves,[4] Rolstad et al.,[5] and Marlowe[11] to relate densification to burnup.

Collins and Hargreaves[4] suggested, and Burton and Reynolds[9] showed, for at least thermal sintering, that a complete description of UO_2 fuel densification requires knowledge of the pore size distribution and the associated pore volumes. The work performed by Marlowe[11] also suggested that grain size and grain growth parameters may affect the densification rate. However, no material characterization (porosity distribution, grain size, pore morphology, etc.) of the fuel used in any of the irradiated tests was reported. Therefore, no quantitative relationships between densification and material properties can be developed in spite of the arguments by Collins and Hargreaves,[4] Ferrari et al.,[7] Heal et al.,[8] and Marlowe[11] that the material characteristics influence the in-reactor densification rate.

The relation between densification and burnup suggested by Rolstad successfully describes the burnup dependence of both the original Rolstad et al. data and EPRI data. Since EPRI has shown a threefold increase in densification of fuel above 1000 K, compared with that of fuel below 1000 K, this change in densification rates must be taken into account in the Rolstad model. The NRC model[14] predicts higher densification rates than either the Halden or EPRI data. The Rolstad model successfully provides the in-pile densification dependency on burnup, and the EEI/EPRI results establish maximum densification limits which can be obtained from out-of-pile resintering tests and used in the Rolstad model.

The EEI/EPRI study shows that in-pile densification is dependent on fuel pore size, grain size, and initial porosity. In addition, out-of-pile resintering tests can be used to estimate in-pile densification. The EPRI results also show that out-of-pile resintering tests at 1973 K for 14 h can be used to estimate in-pile densification.

OUT-OF-PILE THERMAL DENSIFICATION OF LOFT UO_2 FUEL

The densification study conducted by EEI/EPRI[12] provided the basis for estimating in-pile densification of LOFT fuel from out-of-pile resintering tests. In the EEI/EPRI study, three combinations of temperature and time were all found equivalent (within ±0.66% TD) to in-pile densification at a fission rate of 1.3×10^{13} fissions/cm^3•s for 1629 h (~3000 MWd/MtU). These temperatures and times are 1537 K for 1500 h, 1873 K for 48 h, and 1973 K for 14 h. The combination of 1973 K for 14 h was selected as a best-estimate for the resintering of LOFT pellets. Resintering for 24 h was also performed for an evaluation by NRC guidelines.[14]

The resintering tests were performed at the INEL. Fuel pellets from LOFT Lots 20-3 and 20-5 were sintered in a Brew furnace in an argon-6% hydrogen mixture at 1973 K for 14 and 24 h. The pellets were heated and cooled at a rate not exceeding 200 K/h. Details of the resintering procedure are presented in Appendix A. The furnace and sample temperatures were measured with a Type C, W-5% Re/W-26% Re thermocouple (the thermocouple calibration data are presented in Appendix B). The resintering test procedure and resintering test results from the study of UO_2 fuel densification in LOFT are summarized in the following subsections.

Resintering Test Procedure

Pellets were selected from Lots 20-3 and 20-5 for the resintering tests because pellets from these lots were used in the first LOFT center fuel bundle. The LOFT pellets were fabricated by blending 0.3% sterotex as a lubricant with the UO_2 powder and pressing the powder into pellets. The pellets from Lots 20-3 and 20-5 were initially sintered at 1798 and 1823 K, respectively, for 3 h, 45 s. Pellets from Lots 20-3 and 20-5 were 0.9271 cm in diameter and 1.5240 cm long and were nominally 92.5% TD and 91.8% TD (TD is 10.96 g/cc), respectively. The oxygen-uranium ratio for the fuel pellets from both lots was 2.001.

In contrast to the LOFT pellet characterization, pellets used in the LOFT Lead Rod Tests,[15] which provided data used to predict LOFT fuel behavior, were stable fuel (with an average densification of about 1% TD) and were fabricated in a manner similar to LOFT pellets except that they were blended with 0.1% zinc sterate as a lubricant, in addition to the sterotex pore former, and sintered at 1923 K for 4 h, compared with 1823 K for 3 h, 45 s for Lot 20-5 pellets. The final as-fabricated density was 91.69% TD.

Two groups of five pellets each from Lot 20-3 were resintered at 1973 K for 14 h and for 24 h, respectively. In addition, six pellets from Lot 20-3 remaining after metallography following the 14 h resinter were, in turn, resintered for an additional 10 h for a total of 24 h at 1973 K. For Lot 20-5, one sample group of 21 pellets was resintered for 14 h at 1973 K and one group of 20 pellets was resintered for 24 h at 1973 K.

The pellet immersion density and dimensions were determined for each pellet before and after sintering. The pellets were dried at 473 K for 1 h in an argon atmosphere. The pellets were weighed in air, W_d, and in water, W_I, with one to two drops of photoflow wetting agent per 100 mL H_2O. The saturated weight, W_s, was obtained by removing the excess water from the pellet surface by rolling a pellet on a lint-free towel saturated with water.

The pellet immersion density was calculated using Equation (3):

$$D_p = \frac{W_d}{W_s - W_I} \cdot D_{H_2O} \qquad (3)$$

where D_p is the immersion density, and D_{H_2O} is the density of water. The other terms were defined in the preceding discussion.

Resintering Test Results

The densification results from the resintering tests of LOFT fuel pellets are characterized by the density and physical measurements. These results are discussed in the following subsections.

Lot 20-3 Pellets. The properties of the as-received pellets and the changes resulting from resintering at 1973 K for 14 and 24 h are described in this section.

The density of each pellet prior to resintering at 1973 K is shown in Table 1. The densities vary between 10.0952 g/cc (92% TD) to 10.1922 g/cc (92.99% TD) with an average of 10.1357 ± 0.0310 g/cc (92.47 ± 0.28% TD), which is the lower limit of the specified density of 94 ± 1.5% TD for the LOFT pellets. The pellet dimensions are also listed in Table 1. Since these pellets were centerless ground, the pellet diameters were uniform with an average value of 0.9295 ± 0.0002 cm. This uniformity should provide a good basis for comparing resintered diameters with initial diameters. Slightly more variation was found with the pellet lengths. The average pellet length was 1.5409 ± 0.0073 cm.

The densities of pellets resintered at 1973 K for 14 h are listed in Table 2. The density increased to 10.4862 g/cc or 95.68% TD. This density increase represents a volume decrease of 3.21%.

From the decrease in density, assuming an isotropic pellet, an average change of 1.07% in pellet dimensions would be expected. The length and diameter of the pellets after resintering are listed in Table 3. The pellet diameter decreased an average of 1.07%, and the pellet length decreased an average of 1.23%. The pellet shrinkage is slightly anisotropic, that is, unequal in different pellet directions.

Table 1. Density and dimensions of pellets from Lot 20-3 prior to resintering

Pellet	Density ±0.01 (g/cc)	Density (% TD)	Diameter ±0.0003 (cm)	Length ±0.0003 (cm)
1	10.1510	92.62	0.9299	1.5545
2	10.1494	92.60	0.9294	1.5474
3	10.1354	92.48	0.9296	1.5420
4	10.1045	92.19	0.9294	1.5359
5	10.0952	92.11	0.9294	1.5326
6	10.1922	92.99	0.9296	1.5469
7	10.1819	92.90	0.9294	1.5423
8	10.1242	92.37	0.9296	1.5436
9	10.1389	92.51	0.9294	1.5352
10	10.1289	92.42	0.9296	1.5380
11	10.1447	92.56	0.9294	1.5537
12	10.1513	92.62	0.9296	1.5420
13	10.1084	92.23	0.9291	1.5372
14	10.0964	92.12	0.9296	1.5364
15	10.1141	92.28	0.9294	1.5331
16	10.1226	92.36	0.9294	1.5491
17	10.0981	92.14	0.9294	1.5448
18	10.1004	92.16	0.9296	1.5410
19	10.1640	92.74	0.9294	1.5359
20	10.1820	92.90	0.9296	1.5255
Average	10.134	92.4650	0.9295	1.5409
Standard deviation	±0.0302	±0.276	±0.00016	±0.0073

Table 2. Densification after resintering pellets from Lot 20-3 at 1973 K for 14 h

Pellet	Density ±0.01 (g/cc)	Density (% TD)	Density Change (g/cc)	Density Change (% TD)
1	10.4623	95.46	0.3113	2.84
2	10.4873	95.69	0.3379	3.08
3	10.4749	95.57	0.3395	3.09
4	10.4575	95.42	0.3530	3.22
5	10.4900	95.71	0.3948	3.60
6	10.5029	95.83	0.3107	2.83
7	10.4944	95.75	0.3125	2.85
8	10.4686	95.52	0.3444	3.15
9	10.5139	95.93	0.3750	3.42
10	10.5103	95.90	0.3814	3.48
Average	10.4862	95.68	0.3461	3.157
Standard deviation	±0.0198	±0.18	±0.0302	±0.276

Table 3. Changes in dimensions afte resintering pellets from Lot 20-3 at 1973 K for 14 h

Pellet	Diameter ±0.0003 (cm)	Change (%)	Length ±0.0003 (cm)	Change (%)
1	0.9202	-1.038	1.5357	-1.209
2	0.9195	-1.066	1.5286	-1.215
3	0.9195	-1.093	1.5225	-1.268
4	0.9202	-0.984	1.5182	-1.158
5	0.9195	-1.066	1.5138	-1.226
6	0.9208	-0.956	1.5291	-1.149
7	0.9195	-1.066	1.5235	-1.219
8	0.9187	-1.175	1.5235	-1.300
9	0.9197	-1.066	1.5171	-1.175
10	0.9190	-1.148	1.5171	-1.354
Average	0.9197	-1.066	1.5230	-1.227
Standard deviation	±0.0005	±0.066	±0.0066	±0.0643

After resintering the pellets at 1973 K for 24 h (see Table 4), only slight increases in pellet density were found, compared with that from resintering at 1973 K for 14 h. The average density after 24 h increased to 10.5224 g/cc (96.01% TD) compared with an average density of 10.4862 g/cc (95.68% TD) after 14 h. This represents only a 0.33% TD increase for an almost twofold increase in time at temperature.

The dimensional measurements are listed in Table 5 for this 24-h resinter. Slight decreases in both diameter and axial length are observed for the 24-h resinter. As with the 14-h resinter, the dimensional changes were anisotropic.

In conclusion, resintering Lot 20-3 at 1973 K for 14 h resulted in a density increase of 3.16% TD, and increasing the resintering time to 24 h resulted in a density increase of 3.62% TD, an increase of 0.46% TD compared with the 14-h resinter. The density increase at 24 h is significantly different than the increase at 14 h. The upper one-sided 95/95 tolerance limit for the density change after resintering at 24 h is 4.37% of TD. According to NRC guidelines this lot would be classified as unstable fuel.[14]

Lot 20-5 Pellets. The properties of the as-received pellets from Lot 20-5 and the changes resulting from resintering at 1973 K for 14 and 24 h are described in this section.

The density and dimensions of each pellet prior to resintering at 1973 K is shown in Table 6. The immersion densities vary from 9.9824 g/cc (91.32% TD) to 10.1819 g/cc (92.90% TD), with an average of 10.0605 g/cc or 91.79% TD. This

Table 4. Density changes after resintering pellets from Lot 20-3 at 1973 K for 24 h

	Density		Density Change	
Pellet	±0.01 (g/cc)	(% TD)	(g/cc)	(% TD)
11	10.5071	95.87	0.3624	3.31
12	10.5207	95.99	0.3694	3.37
13	10.4952	95.76	0.3868	3.53
14	10.5300	96.08	0.4336	3.96
15	10.5225	96.01	0.4084	3.73
16	10.5574	96.33	0.4348	3.97
17	10.5135	95.93	0.4154	3.79
18	10.5233	96.02	0.4229	3.86
19	10.5363	96.13	0.3723	3.39
20	10.5162	95.95	0.3342	3.05
3	10.4906	95.72	0.3552	3.24
4	10.5306	96.08	0.4261	3.89
5	10.5187	95.97	0.4235	3.86
8	10.5493	96.25	0.4251	3.88
9	10.5124	95.92	0.3735	3.41
10	10.5348	96.12	0.4059	3.70
Average	10.5224	96.01	0.3968	3.62
Standard deviation	±0.0176	±0.16	±0.0319	±0.29

Table 5. Dimensional measurements after resintering pellets from Lot 20-3 at 1973 K for 24 h

Pellet	Diameter ±0.0003 (cm)	Change (%)	Length ±0.0003 (cm)	Change (%)
11	0.9190	-1.12	1.5339	-1.27
12	0.9195	-1.09	1.5215	-1.33
13	0.9190	-1.11	1.5171	-1.31
14	0.9185	-1.22	1.5156	-1.35
15	0.9182	-1.20	1.5126	-1.34
16	0.9191	-1.11	1.5281	-1.36
17	0.9190	-1.11	1.5230	1.41
18	0.9182	-1.23	1.5199	1.37
19	0.9188	-1.14	1.5156	1.32
20	0.9190	-1.14	1.5065	1.25
3	0.9190	-1.14	1.5199	1.43
4	0.9190	-1.12	1.5161	1.29
5	0.9190	-1.12	1.5126	1.30
8	0.9182	-1.23	1.5222	1.39
9	0.9192	-1.10	1.5159	1.26
10	0.9177	-1.28	1.5164	1.40
Average	0.9188	1.15	1.5186	1.34
Standard deviation	±0.00048	±0.058	±0.0065	±0.056

density is slightly less than that of Lot 20-3, although this lot was initially sintered at a slightly higher temperature (1823 K) for the same time (3 h, 45 s). Prior to resintering, the average pellet diameter was 0.9299 ± 0.0004 cm and the average pellet length was 1.5360 ± 0.1112 cm.

The immersion densities of the pellets sintered at 1973 K for 14 h are listed in Table 7. The density average increased to 10.463 g/cc or 95.47% TD. This density increase results in a density change average of 3.68% TD, which is slightly higher than that of Lot 20-3.

The diameter and length of Lot 20-5 pellets after resintering for 14 h at 1973 K are listed in Table 8. The average decrease in diameter is 1.23%, and the average decrease in length is 1.35%. These values still show some anisotropic behavior in the densification of Lot 20-5 pellets.

Resintering these pellets an additional 10 h (a total of 24 h) at 1973 K caused the average density shown in Table 9 to decrease to 10.4372 g/cc (95.23% TD) from 10.4658 g/cc (95.49% TD) after the 14-h resinter. The average diameter increased slightly as a result of the additional 10-h resinter at 1973 K (see Table 10).

In conclusion, resintering Lot 20-5 at 1973 K for 14 h resulted in an increase of 3.68% TD; but after resintering for 24 h, the density increase was only 3.40% TD, a decrease of 0.28% TD. This decrease is significant, and may result from swelling during pore coalescence when the pore pressure is in equilibrium with the surface tension.[16] Similar swelling was noted during grain growth of irradiated UO_2.[17] The upper one-sided 95/95 tolerance limit for the density change after resintering for 24 h is 4.38% TD, which results in classifying this lot as unstable fuel according to NRC guidelines.[14]

Table 6. Density and dimensions of pellets from Lot 20-5 prior to resintering

Pellet	Density (g/cc)	Density (% TD)	Diameter (cm)	Length (cm)
1	10.1819	92.90	0.9301	1.5494
2	10.1473	92.58	0.9301	1.5143
3	10.1106	92.25	0.9304	1.5486
4	10.0668	91.85	0.9301	1.5313
5	10.0963	92.12	0.9296	1.5342
6	10.0738	91.91	0.9301	1.5519
7	10.0090	91.32	0.9296	1.5268
8	10.0893	92.06	0.9301	1.5334
9	10.0587	91.78	0.9304	1.5431
10	10.0465	91.67	0.9301	1.5268
11	10.0117	91.35	0.9296	1.5410
12	10.0489	91.69	0.9296	1.5306
13	10.0571	91.76	0.9299	1.5194
14	10.0507	91.70	0.9296	1.5456
15	10.0447	91.64	0.9304	1.5362
16	10.0440	91.40	0.9301	1.5329
17	10.0261	91.46	0.9299	1.5372
18	10.0235	91.72	0.9296	1.5301
19	10.0529	91.69	0.9296	1.5560
20	10.0489	91.08	0.9291	1.5471
21	9.9824	91.79	0.9294	1.5210
Average	10.0605	91.79	0.9299	1.5360
Standard deviation	±0.0458	±0.42	±0.00036	±0.0112

Statistical Analyses. Statistical analyses were performed to determine

1. Whether the standard deviations of parameters are statistically the same for different resintering times and for different lots
2. Whether there are any statistically significant differences in pellet parameters from different lots, but for the same resintering time
3. The tolerance limits for each pellet parameter.

Table 11 summarizes the standard deviations for density, diameter, and length derived from the resintering data of Lots 20-3 and 20-5. Within the individual lots, the standard deviations for the three parameters after resintering for 14 and 24 h are not significantly different, but there is a difference between standard deviation for density and diameter for the as-received and resintered pellets. The length standard deviation does not change after resintering from the as-received pellets. Between lots, parameter standard deviations after resintering times of 14 and 24 h are different for density and length, but not for diameter. Also, the standard deviations of each parameter for unresintered pellets varies

Table 7. Densification after resintering pellets from Lot 20-5 at 1973 K for 14 h

Pellet	Density ±0.01 (g/cc)	Density (% TD)	Density Change (g/cc)	Density Change (% TD)
1	10.4648	95.48	0.2829	2.58
2	10.4591	95.43	0.3118	2.84
3	10.4839	95.66	0.3733	3.41
4	10.4879	95.69	0.4211	3.84
5	10.4168	95.04	0.3205	2.92
6	10.4937	95.75	0.4199	3.83
7	10.4776	95.60	0.4686	4.28
8	10.4538	95.38	0.3645	3.33
9	10.4796	95.62	0.4209	3.84
10	10.4606	95.44	0.4141	3.78
11	10.4092	94.97	0.3975	3.63
12	10.4591	95.43	0.4102	3.74
13	10.4629	95.46	0.4058	3.70
14	10.4785	95.61	0.4278	3.90
15	10.4916	95.73	0.4469	4.08
16	10.4466	95.32	0.4026	3.67
17	10.4689	95.52	0.4428	4.04
18	10.3721	94.64	0.3486	3.18
19	10.4933	95.74	0.4404	4.02
20	10.4823	95.64	0.4334	3.95
21	10.4899	95.71	0.5075	4.63
Average	10.463	95.47	0.4029	3.68
Standard deviation	±0.0310	±0.28	±0.0537	±0.4900

significantly between the two lots. The standard deviation of 5.86×10^{-4} cm for diameter in Table 11 results from pooling the sample standard deviations from both Lots 20-3 and 20-5 for the 14- and 24-h treatments. The standard deviations for density were only pooled within each lot for the 14- and 24-h treatments, resulting in 0.0188 g/cc for Lot 20-3 and 0.0292 g/cc for Lot 20-5; however, the standard deviations for length from the as-received samples were pooled with the 14- and 24-h treatments, resulting in 6.92×10^{-3} cm for Lot 20-3 and 11.3×10^{-3} cm for Lot 20-5.

Resintering at 1973 K for either 14 or 24 h results in the density standard deviation decreasing significantly, and the diameter standard deviation increasing significantly. The length standard deviation is unaffected. These results suggest that pellet lengths decrease uniformly and the pellet diameters decrease sporadically.

The average of the parameters for the different lots and resintering times are shown in Table 12. For a resintering time of 14 h, the density and length of Lot 20-3 are significantly different than those of Lot 20-5, but the diameters for both lots are the same. For 24 h, a significant difference between lots appears only in density, while the diameter and length have reached parity. The density increase occurring in Lot 20-3 from increasing the sintering time from 14 h to 24 h is statistically

Table 8. Changes in dimensions after resintering pellets from Lot 20-5 at 1973 K for 14 h

Pellet	Diameter (cm)	Change (%)	Length (cm)	Change (%)
1	0.9200	-1.09	1.5281	-1.37
2	0.9192	-1.17	1.4923	-1.45
3	0.9205	-1.06	1.5291	-1.26
4	0.9197	-1.12	1.5098	-1.40
5	0.9195	-1.09	1.5093	-1.62
6	0.9200	-1.09	1.5339	-1.16
7	0.9190	-1.14	1.5047	-1.45
8	0.9200	-1.09	1.5121	-1.39
9	0.9202	-1.10	1.5225	-1.33
10	0.9190	-1.19	1.5085	-1.20
11	0.9192	-1.12	1.5014	-2.57
12	0.9187	-1.17	1.5080	-1.48
13	0.9195	-1.12	1.5331	+0.90
14	0.9185	-1.19	1.5250	-1.33
15	0.9187	-1.26	1.5179	-1.19
16	0.9197	-1.12	1.5141	-1.23
17	0.9190	-1.17	1.5197	-1.14
18	0.9192	-1.12	1.5103	-1.29
19	0.9192	-1.12	1.4994	-3.64
20	0.9195	-1.03	1.5243	-1.47
21	0.9197	-1.04	1.5159	-0.34
Average	0.9194	-1.23	1.5152	-1.35
Standard deviation	±0.00035	±0.0547	±0.0113	±0.8095

significant, just as the density decrease in Lot 20-5 is significant from the increase in sintering time. These results suggest that for Lot 20-5, the pore pressure may be in equilibrium with surface tension so that volume expansion occurs upon bubble coalescence.[16,17]

Table 12 also lists the 95/95 two-sided tolerance limits based on an assumed Gaussian distribution. This assumption allows a higher probability for a small number of degrees of freedom.

A statistical analysis of the resintering data shows that the diameters from Lots 20-3 and 20-5 could be pooled for each of the resintering times of 14 and 24 h, and only the length from Lots 20-3 and 20-5 could be pooled for the 24-h resinter.

Anisotropic behavior occurred in the changes in the dimensional measurements for both Lots 20-3 and 20-5. After resintering for 24 h, the decrease in length was 15 to 19% greater than the change in diameter.

Table 9. Density changes after resintering pellets from Lot 20-5 at 1973 K for 24 h

Pellet	Density (g/cc)	Density (% TD)	Density Change (g/cc)	Density Change (% TD)
1	10.4508	95.35	0.2689	2.45
2	10.4192	95.07	0.2719	2.48
3	10.4718	95.55	0.3612	3.30
4	10.4603	95.44	0.3935	3.59
5	10.4692	95.52	0.3729	3.40
6	10.4641	95.48	0.3903	3.56
7	10.4489	95.34	0.4399	4.01
8	10.4274	95.14	0.3381	3.08
9	10.4615	95.45	0.4028	3.68
10	10.4354	95.21	0.3889	3.54
11	10.3776	94.69	0.3659	3.34
12	10.3904	94.80	0.3415	3.11
13	10.4120	95.00	0.3549	3.24
14	10.4111	94.99	0.3604	3.29
15	10.4521	95.37	0.4074	3.72
16	10.4063	94.95	0.3623	3.31
17	10.4647	95.48	0.4386	4.00
18	10.4418	95.27	0.4183	3.82
19	10.4480	95.33	0.3951	3.60
20	10.4308	95.17	0.3819	3.48
Average	10.4372	95.23	0.3727	4.40
Standard deviation	±0.0271	±0.25	±0.0450	±0.4107

Table 10. Dimensional measurements after resintering pellets from Lot 20-5 at 1973 K for 24 h

Pellet	Diameter (cm)	Change (%)	Length (cm)	Change (%)
1	0.9190	-1.19	1.5268	-1.46
2	0.9190	-1.19	1.4910	-1.54
3	0.9195	-1.17	1.5265	-1.43
4	0.9195	-1.14	1.5121	-1.25
5	0.9182	-1.23	1.5123	-1.43
6	0.9192	-1.17	1.5301	-1.40
7	0.9177	-1.28	1.5022	-1.61
8	0.9192	-1.17	1.5108	-1.47
9	0.9195	-1.17	1.5215	-1.40
10	0.9177	-1.33	1.5062	-1.35
11	0.9190	-1.14	1.5138	-1.77
12	0.9185	-1.19	1.5080	-1.48
13	0.9185	-1.23	1.4966	-1.50
14	0.9185	-1.19	1.5263	-1.25
15	0.9185	-1.28	1.5174	-1.22
16	0.9185	-1.25	1.5123	-1.34
17	0.9182	-1.26	1.5141	-1.50
18	0.9172	-1.33	1.5055	-1.61
19	0.9185	-1.19	1.5324	-1.52
20	0.9174	-1.26	1.5260	-1.36
Average	0.918	-1.22	1.5146	-1.45
Standard deviation	±0.00069	±0.0572	±0.0113	±0.132

Table 11. Estimated standard deviations of parameter populations with degrees of freedom

Parameter	Resintering Time (h) 0	14	24
Lot 20-3			
Density (g/cc)	0.0302 (19)[a]	0.0188 (23)	0.0188 (23)
Diameter (cm x 10^4)	1.62 (19)	5.85 (62)	5.86 (62)
Length (cm x 10^3)	6.92 (42)	6.92 (42)	6.92 (42)
Lot 20-5			
Density (g/cc)	0.0458 (20)	0.0292 (39)	0.292 (39)
Diameter (cm x 10^4)	3.56 (20)	5.86 (62)	5.86 (62)
Length (cm x 10^3)	11.3 (47)	11.3 (59)	11.3 (59)

a. Numbers in parentheses denote degrees of freedom.

Table 12. Tolerance limits[a]

Parameter	14-h Resinter			24-h Resinter		
	Lower	Average	Upper	Lower	Average	Upper
Lot 20-3						
Density (g/cc)	10.4344	10.4862	10.5380	10.4706	10.5224	10.5742
Diameter (cm)[b]	0.9181	0.9195	0.9209	0.9173	0.9187	0.9200
Length (cm)	1.5055	1.5230	1.5405	1.4902	1.5166[c]	1.5430
Lot 20-5						
Density (g/cc)	10.3910	10.4634	10.5359	10.3647	10.4372	10.5097
Diameter (cm)[b]	0.9181	0.9195	0.9209	0.9173	0.9187	0.9200
Length (cm)	1.4885	1.5360	1.5419	1.4902	1.5166[c]	1.5430

a. Probability is 0.95 that 95% of population is within limits; Gaussian distribution assumed.

b. Lot averages not significantly different at each resintering time. Variances are pooled.

c. Lot averages not significantly different at 24-h resintering time. Variances significantly different. Larger variance used for tolerance limits.

PORE SIZE AND MICROSTRUCTURE CHARACTERIZATION OF LOFT FUEL PELLETS

The as-received and resintered LOFT fuel pellets from Lots 20-3 and 20-5 were characterized with respect to their microstructure and porosity distribution. The pellet characterization procedure and characterization results are summarized in the following subsections.

Pellet Characterization Procedure

Transverse and longitudinal cross sections were obtained from the as-received pellets and pellets heated at 1973 K for 14 and 24 h. Two transverse sections were prepared from an as-received pellet from Lot 20-3: one section at the center of the pellet and the other section near the end of the pellet to determine porosity variations at different locations in the pellet. The longitudinal sections taken from the as-received and resintered pellets also give some insight into the porosity variations. For Lot 20-5, cross sections were taken near the center and end of each pellet.

The pore size and pore size distributions were obtained from optical metallography using a Bausch and Lomb image analyzer. The details of the pore size characterization procedure are given in Appendix C. Pore volumes were calculated on the assumption of spherical pores. Grain size measurements were obtained from etched samples using the linear intercept method.

Pellet Characterization Results

Microstructures and the pore size distributions derived from the microstructures for pellets from Lots 20-3 and 20-5 are described in this section.

Microstructure and Pore Size Distribution from Lot 20-3. Views (a) and (b) in Figure 4 show typical microstructures of the as-received LOFT fuel pellets from Lot 20-3. The porosity distribution is very heterogeneous. Most of the porosity is clustered in localized areas appearing as dark patches. Other areas contain localized porosity-free zones with grain sizes of about 5.5 μm, compared with a 3.5-μm grain size in the remainder of the cross section.

Pore sizes and pore size distributions determined metallographically for different areas in a pellet are shown in Figure 5. A large fraction of the porosity is between 7 and 20 μm, which is the size range for densification. The remaining porosity exceeds 80 μm, originating from only a few, very large pores, or is less than 1 μm for many small pores. The former are expected to be very stable. The porosity volumes derived from the pore size distributions are listed in Table 13 for different areas of the as-received pellet. The porosity volume at the center of the pellet varies from 7.29 to 7.82%, with an average of 7.51%, compared with an average of 7.53% from immersion densities. The porosity at the end of the pellet is less than the center, varying from 4.18 to 5.66%, with an average of 4.78%.

Figure 6 shows a typical microstructure of a pellet resintered at 1973 K for 14 h. The structure has become more homogeneous than that of the as-received material. The fine porosity is located primarily within the grains with a few large isolated pores at the grain boundaries. The grain size increased from 3.5 to 12.2 μm after heating at 1973 K for 14 h.

A typical pore size distribution is shown in Figure 7 for the pellets sintered at 1973 K for 14 h. In comparison with the as-received material, the greatest reduction of 50% in pore volume occurred for pores between 1 and 35 μm, with smaller reductions (~25%) from pores between 0.02 and 0.1 μm. Pores above 80 μm were little affected by the resintering. The pore volume calculated for different areas in a pellet varied from 4.08 to 4.61% with an average of 4.38%. This value compares quite well with the value of 4.32% determined from immersion densities.

A typical microstructure is shown in Figure 8 for pellets resintered at 1973 K for 24 h. The structure is very similar to that from the 14-h resinter, except the grain size has increased to 17.6 μm.

The porosity distribution shown in Figure 9 is very similar to that for the 14-h resinter. Most of the reduction in pores is between 7 and 30 μm (~60%), with most of the remaining porosity arising from the large pore sizes.

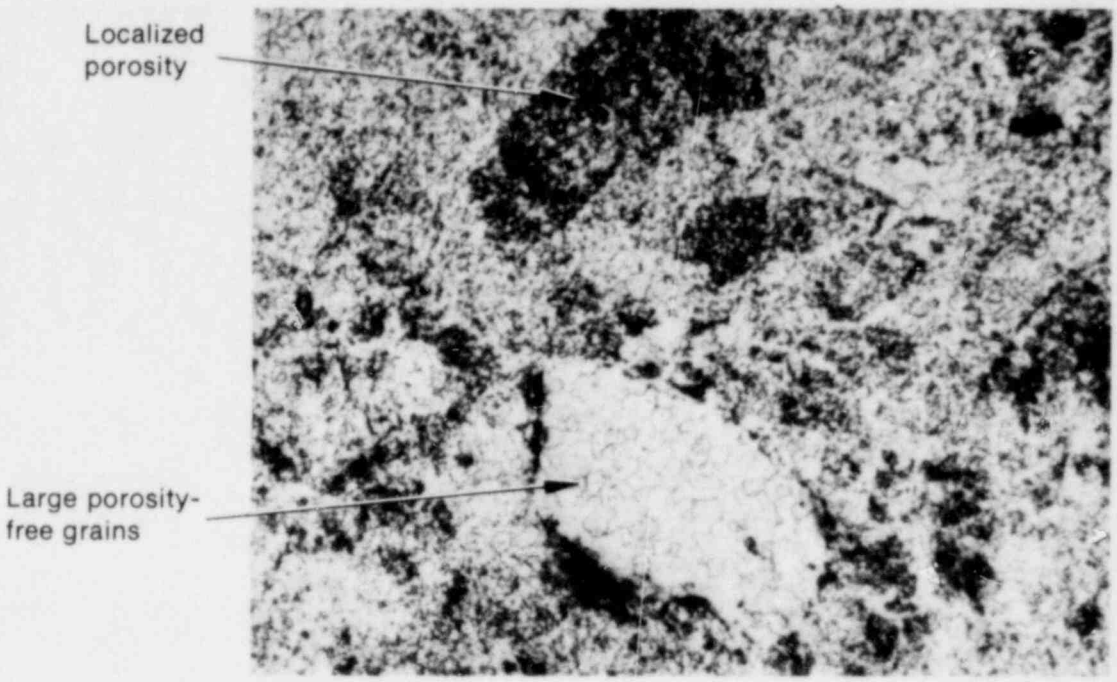

View (a)

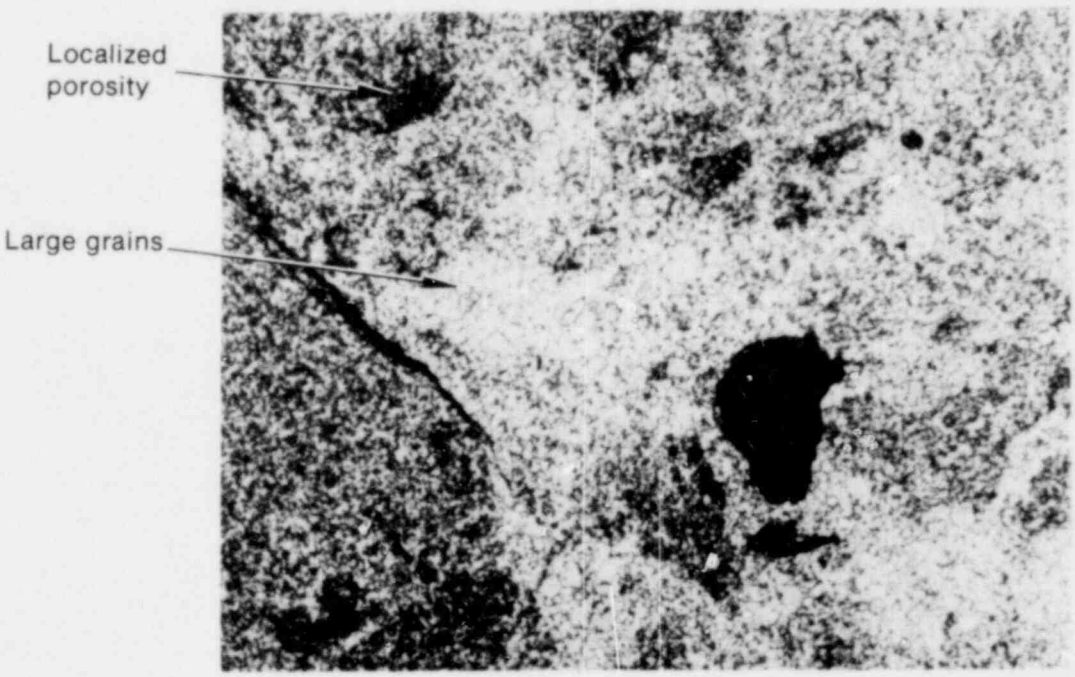

INEL-A-11 166

View (b)

Figure 4. Typical microstructure of as-received UO_2 pellets from Lot 20-3.

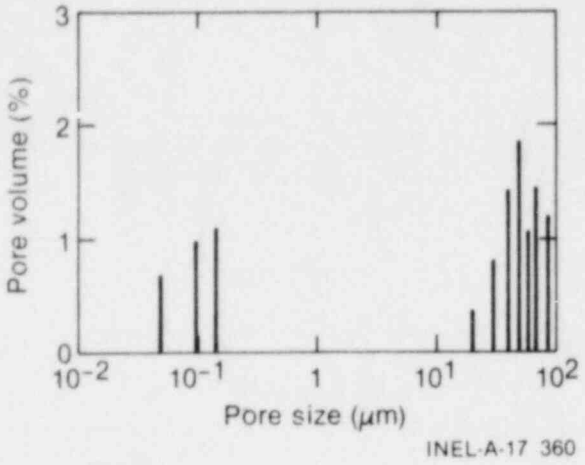

Figure 5 Pore volume distribution for as-received UO_2 pellets from Lot 20-3.

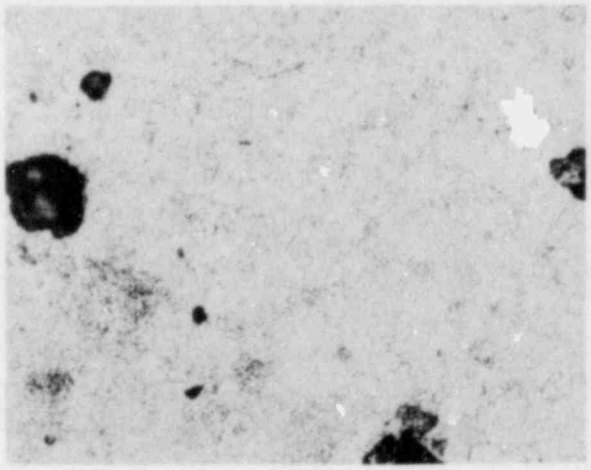

Figure 6. Typical microstructure of UO_2 pellets from Lot 20-3 after resintering at 1973 K for 14 h.

Table 13. Porosity volume for different areas of as-received pellets from Lot 20-3

Pore Size (μm)	Porosity at Center of Pellet (%)		
	Outer Edge	Midradius	Center
Less than 1	1.86	3.98	3.32
Between 1 and 40	2.63	1.95	1.30
Greater than 40	2.79	1.89	2.79
Total	7.28	7.82	7.41

Pore Size (μm)	Porosity at End of Pellet (%)		
	Outer Edge	Midradius	Center
Less than 1	3.43	2.49	2.27
Between 1 and 25	1.09	0.81	0.86
Greater than 25	1.14	0.88	1.37
Total	5.66	4.18	4.50

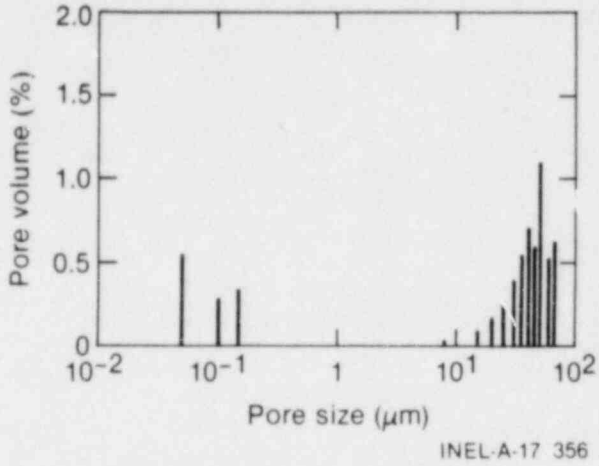

Figure 7. Pore volume distribution for UO_2 pellets from Lot 20-3 resintered at 1973 K for 14 h.

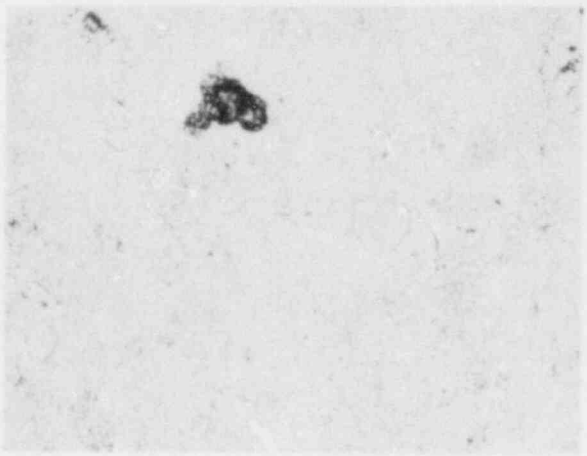

Figure 8. Typical microstructure of UO_2 pellets from Lot 20-3 after resintering at 1973 K for 24 h.

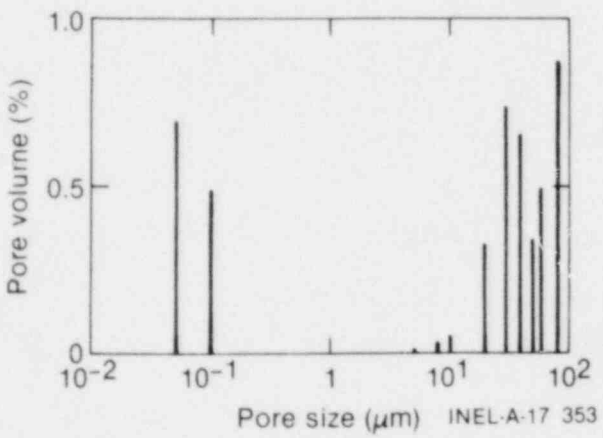

Figure 9. Pore volume distribution for UO_2 pellets from Lot 20-3 resintered at 1973 K for 24 h.

The total porosity determined from metallography for different areas in a pellet varies from 2.62 to 5.01%, with an average of 4.04%. This value is quite consistent with the 4.06% volume porosity determined from the immersion densities.

Microstructure and Pore Size Distribution from Lot 20-5. Figure 10 shows the typical microstructure of the as-received pellets from Lot 20-5. The microstructure is very similar to that of pellets from Lot 20-3. Most of the porosity is clustered in localized areas appearing as dark patches. The grain size is more uniform than the grain size of Lot 20-3, averaging about 3.6 μm.

Pore sizes and pore size distributions determined metallographically for different areas in a pellet are shown in Figure 11. A large fraction of the porosity (81%) lies between 1 and 10 μm. The porosity volume derived from the pore size distributions are listed in Table 14 for different areas of the as-received pellet. The porosity volume at the center of the pellet varies from 8.43 to 9.20%, with an average of 8.75%. The value of 8.21% from immersion density is fairly consistent with the pore value measurements. The porosity at the end of the pellet is larger than at the center location and varies from 10.67 to 14.97%, with an average of 12.74%.

Figure 12 shows a typical microstructure of a pellet resintered at 1973 K for 14 h. The structure has become more homogeneous than that of the as-received material. The grain size increased from 3.6 to 10.70 μm after heating at 1973 K for 14 h.

A typical pore size distribution is shown in Figure 13 for the pellets resintered at 1973 K for 14 h. The greatest reduction in pore volume occurred for pores between 1 and 10 μm, with smaller reductions for pores less than 1 μm. Pore volumes calculated for different areas in the pellet vary from 5.07 to 8.29%, with an average of 6.76%. This value is higher than the value of 4.53% porosity determined from immersion densities.

A typical microstructure is shown in Figure 14 for pellets resintered at 1973 K for 24 h. The structure is still somewhat heterogeneous, with the porosity scattered in localized clusters. The grain size has now increased to 13.5 μm.

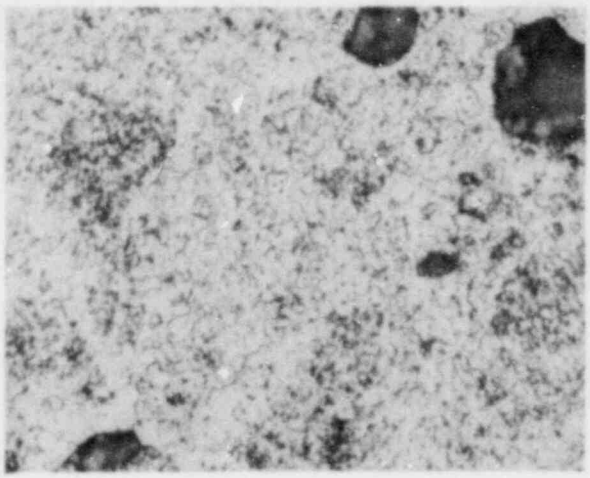

Figure 10. Typical microstructure of as-received UO_2 pellets from Lot 20-5.

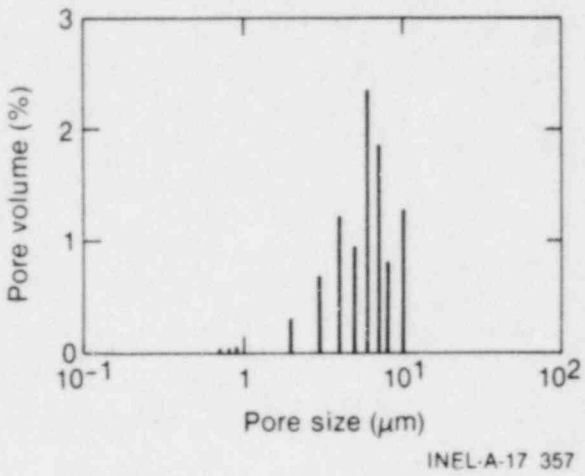

Figure 11. Pore volume distribution for as-received UO_2 pellets from Lot 20-5.

Table 14. Porosity volume for different areas of as-received pellets from Lot 20-5

Pore Size (μm)	Porosity at Center of Pellet (%)		
	Outer Edge	Midradius	Center
Less than 1	1.81	1.22	1.57
Between 1 and 10	6.80	7.98	6.86
Total	8.61	9.20	8.43

Pore Size (μm)	Porosity at End of Pellet (%)		
	Outer Edge	Midradius	Center
Less than 1	1.90	1.54	2.88
Between 1 and 10	13.07	9.13	9.68
Total	14.97	10.67	12.56

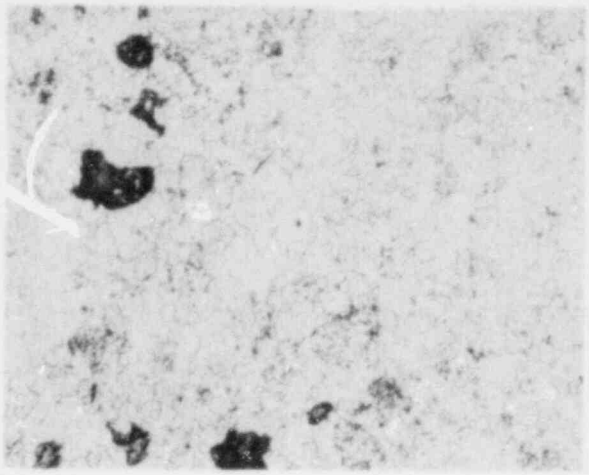

Figure 12. Typical microstructure of UO_2 pellets from Lot 20-5 after resintering at 1973 K for 14 h.

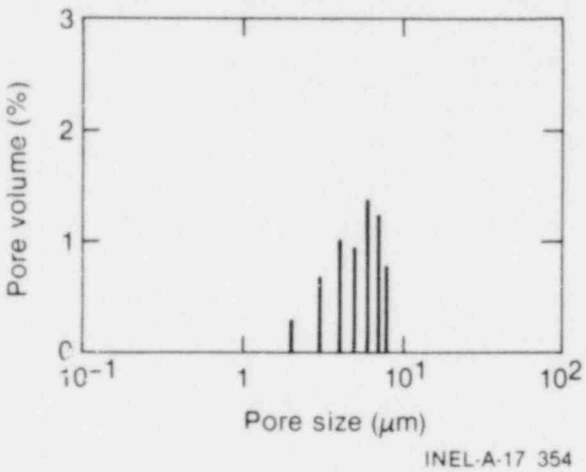

Figure 13. Pore volume distribution for UO_2 pellets from Lot 20-5 resintered at 1973 K for 14 h.

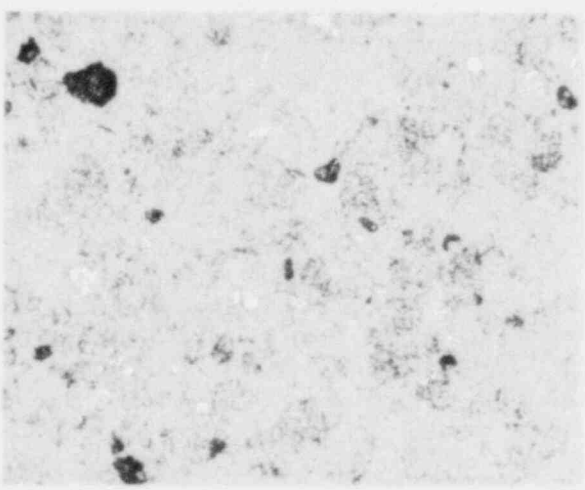

Figure 14. Typical microstructure of UO_2 pellets from Lot 20-5 after resintering at 1973 K for 24 h.

The total porosity, determined by metallography and shown in Figure 15, for different areas in a pellet resintered for 24 h varies from 4.04 to 4.93%, with an average of 4.62%. This value agrees favorably with 4.77% porosity measured by immersion.

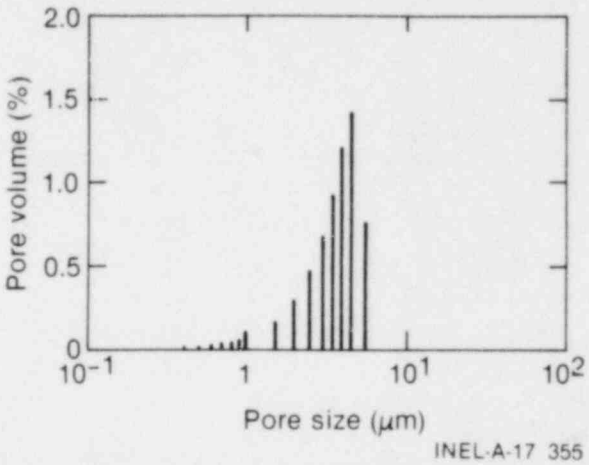

Figure 15. Pore volume distribution for UO_2 pellets from Lot 20-5 resintered at 1973 K for 24 h.

Characterization Results Compared for Lots 20-3 and 20-5. The microstructures for the as-received UO_2 fuel pellets from Lots 20-3 and 20-5 indicate that porosity of the pellets is very heterogeneous. The porosity is scattered and grouped at very localized areas. Other areas show large (5.5 μm), almost porosity-free grains in a matrix of a smaller grained (3.5 μm) material.

Upon resintering the pellets, the greatest reduction in porosity occurs for pores between 1 and about 35 μm for pellets from Lot 20-3 and between 1 and 10 μm for pellets from Lot 20-5. Some pore coalescence occurs for pores less than 1 μm. The UO_2 grain size for Lot 20-3 increases from 3.5 to 12.2 μm after 14 h and to 17.6 μm after 24 h during resintering at 1973 K. For Lot 20-5, the grain size increases to 10.7 μm after 14 h and to 13.5 μm after 24 h during resintering at 1973 K. The smaller increases in grain size in Lot 20-5 compared with Lot 20-3 may be attributed to the preponderence of smaller pores in Lot 20-5. Coalescence of these smaller pores may also cause the slight increase in density after resintering at 24 h.

LOFT FUEL DENSIFICATION AS A FUNCTION OF BURNUP

The density increases of 3.62% TD for Lot 20-3 and 3.40% TD for Lot 20-5 determined from the 24-h out-of-pile resintering test, is the maximum in-pile densification expected to occur. However, the out-of-pile resintering tests were not correlated with a burnup dependency of in-reactor densification because the large number of samples required was too costly. Therefore, a best-estimate model developed for MATPRO[18] and based on in-pile densification was used to derive a burnup dependency for the densification of LOFT fuel. The model requires an estimate of the maximum density change from irradiation; this estimate is used in a densification correlation based on burnup.

The MATPRO model allows a choice between two methods to calculate the maximum density change during irradiation. The preferred method uses the density change determined from a resintering test performed at 1973 K for 24 h. One of two equations may be used, depending on the fuel temperature: if the fuel temperature (T) is below 1000 K, Equation (4) is used; if T is greater than 1000 K, Equation (5) is used:

$$\left(\frac{\Delta L}{L}\right)_{max} = 0.0015\ \Delta P \quad T < 1000\ K \tag{4}$$

$$\left(\frac{\Delta L}{L}\right)_{max} = 0.0285\ \Delta P \quad T \geq 1000\ K \tag{5}$$

where ΔP is the change in density (kg/m^3) from a resintering test and $(\Delta L/L)_{max}$ is the maximum percent of change in radial dimension.

If out-of-pile resintering densification data are not available, the maximum density change is calculated from equations based on Halden in-pile densifications. One of two equations again may be selected, depending on the fuel temperature:

$$\left(\frac{\Delta L}{L}\right)_{max} = \frac{22.2\ (100 - DENS)}{(T_{SINT} - 1453)} \quad T < 1000\ K \tag{6}$$

$$\left(\frac{\Delta L}{L}\right)_{max} = \frac{66.6\ (100 - DENS)}{(T_{SINT} - 1453)} \quad T \geq 1000\ K \tag{7}$$

where T_{SINT} is the sintering temperature (K) and DENS is the fuel density (%TD).

Densification as a function of burnup is calculated according to Equation (8) where the appropriate value of $(\Delta L/L)_{max}$ is selected from Equations (4), (5), (6), or (7):

$$\frac{\Delta L}{L} = -\left(\frac{\Delta L}{L}\right)_{max} + \exp\left[-3.0\ (FBU + B)\right] + 2.0 \exp\left[-35\ (FBU + B)\right] \tag{8}$$

where

$\frac{\Delta L}{L}$ = the percent of change in radial dimension

FBU = fuel burnup ($MWd/kgUO_2$)

B = a constant to fit the boundary condition $\frac{\Delta L}{L} = 0$ when FBU = 0.

The results of calculations using the Halden equations and the out-of-pile experimental resintering density for Lot 20-3 are shown in Figure 16. Curves 1 and 3 are based on the maximum dimensional changes derived from Halden Equations (6) and (7), respectively. Both curves show the maximum density is attained at about 1 $MWd/kgUO_2$ (1134 MWd/MtU). For fuel temperatures less than 1000 K, the maximum change in length is 0.60% from Equation (6), compared with 1.57% from Equation (7) for fuel temperatures above 1000 K. Based on experimental densification, the maximum length change of 1.13% from Equation (5) lies between the two Halden curves. For the case of fuel temperature lying below 1000 K, the densification curve based on resintering is coincident with Curve 1. For the fuel temperatures greater than 1000 K, LOFT fuel densification is expected to follow Equation (5) (Curve 2).

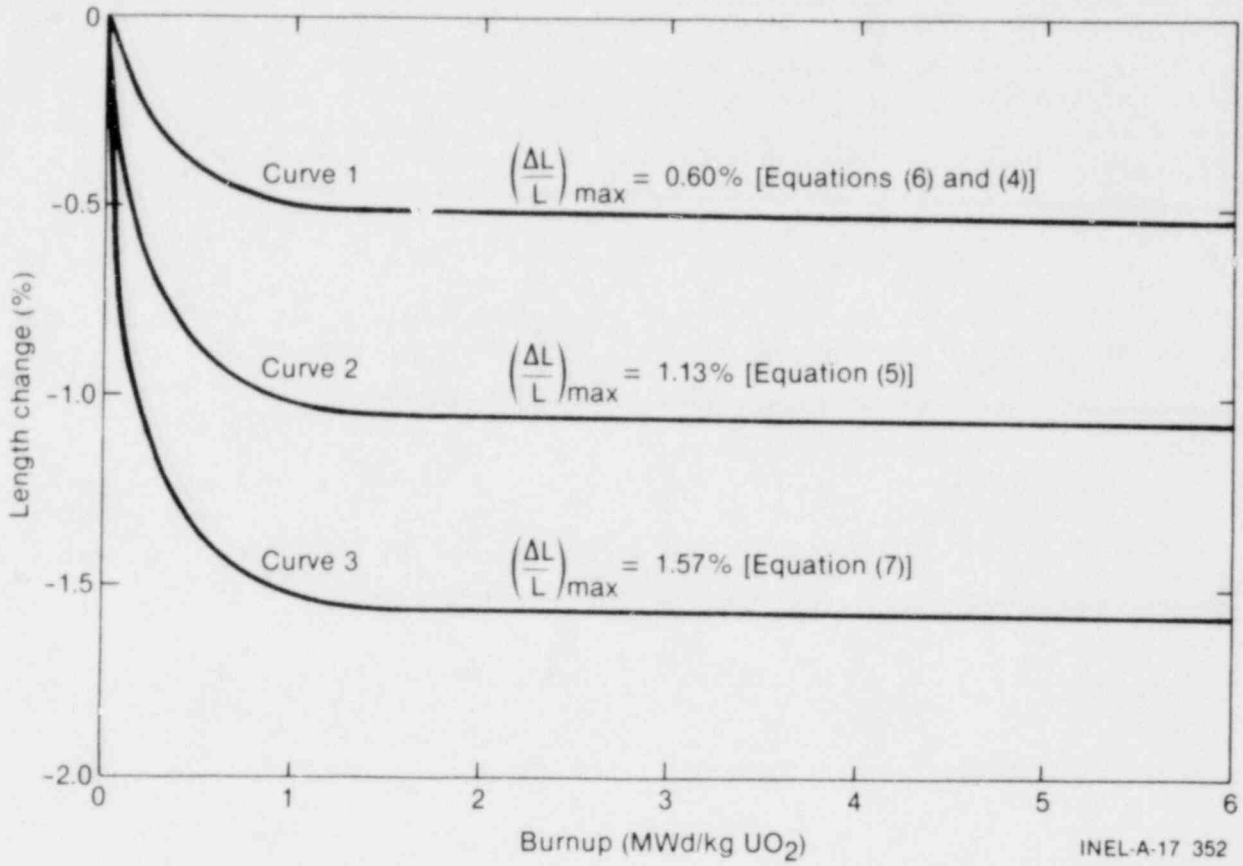

Figure 16. Densification as a function of burnup for different final length changes.

EFFECTS OF Ddensification ON FUEL ROD BEHAVIOR

The effects of densification on fuel behavior during steady-state operation and LOCEs are controversial because of the ambiguous effects of pellet cracking and relocation, cladding creepdown, and axial pellet gaps. The following evaluation is limited to these three effects in order to identify the effect on fuel cladding thermal response caused by changes in fuel dimensions.

Stored Energy

A decrease in pellet diameter increases the gap width and thereby decreases the gap conductance if no cladding collapse occurs. The formation of circumferential cracks in the fuel reduces the decrease in gap width, but these cracks have the same effect of decreasing gap conductance through a reduction in thermal conductivity of the fuel. Also, the decrease in volume increases the volumetric heat generation rate. The decrease in gap conductance, the decrease in thermal conductivity, and the increase in the heat generation rate, increase the stored energy of the UO_2 pellets. This stored energy may be decreased slightly from increased thermal conductivity due to a porosity reduction. FRAP-T5[a,19] calculations were performed to determine the magnitude of changes in stored energy as a result of the above parameters; however, local power peaking due to axial pellet gaps was not considered. This was because of compensating effects of radiation heat loss from the power spikes to adjacent gaps.[20]

Steady-state fuel temperatures and corresponding stored energies were calculated with FRAP-T5[19] using the Ross-Stoute gap conductance model and pellet relocation and thermal properties described in MATPRO-11.[18] For three different power levels (~26.3 kW/m, 39.4 kW/m, and 52.5 kW/m), the steady-state temperature initialization was performed using the nominal dimensions of the LOFT fuel rods and fuel with a 92.36% TD. Each base case calculation was perturbed from using a final pellet diameter of 9.19 mm, which represents complete densification. To facilitate the calculation, the stack height was left unchanged and the lineal power generation rate was increased 1.22% to compensate for the decrease in stack height. The diameter decrease already compensated for the power increase.

The results of the calculations are shown in Table 15. For the power level of 26.3 kW/m, the average fuel temperature increased 141 K, a 12.7% increase. The stored energy increased 19.8% from 240.2 J/g to 286.5 J/g. For the 39.4-kW/m power level, the average fuel temperature increased 126 K (10.9%), with a corresponding 15.0% increase (46.6 J/g) in stored energy. For the 52.5-kW/m power level, the average fuel temperature increased 125 K with an increase of 12.2% (45.7 kJ/g) in stored energy. The large increase in stored energy from as-received to fully densified fuel is due to the higher volumetric power arising from the change in fuel dimensions. The decreasing changes in stored energy with increasing power levels are attributed to a higher gap conductance due to a higher pressure at the UO_2-zircaloy cladding interface.

An example of the effect of the stored energy increase on the cladding temperatures obtained from FRAP-T5 calculations of a LOCE with a 39.4-kW/m power level is shown in Figure 17. In this figure, cladding temperatures as a function of time for three fuel rods with 0, 1, and 3.5% densification, respectively, are compared. The peak cladding temperatures increased 106 K from the undensified fuel to the fuel with maximum densification (~1000 MWd/MtU). This change in cladding temperature is not supported experimentally in the Halden tests,[20] where there was no difference in fuel thermal resistance between densified and undensified fuel. As shown in Figure 17, fuel densified at 1% (stable density fuel) has an increase in cladding temperature of only 10 K.

The increase in stored energy from the maximum densification significantly affects the cladding temperature during a LOCE as shown in Figure 17. A 0.05-mm cladding creepdown with maximum densification results in only a 14-K rise in cladding temperature. The effect of cladding creep nullifies the effect of maximum densification. Local power peaking at axial pellet gaps was not considered in these calculations because the

[a] Idaho National Engineering Laboratory Configuration Control Number HO11685B.

Table 15. Calculated changes in stored energy from densified UO_2 fuel

Peak Power (kW/m)	Average Fuel Temperature (K)	Increase In Fuel Temperature (K)	Increase In Fuel Temperature (%)	Stored Energy (J/g)	Change (%)
26.25	1111			240.2	
		141	12.7		19.3
26.60	1252			286.5	
39.37	1323			310.5	
		136	10.9		15.0
39.90	1459			359.1	
52.49	1509			376.0	
		125	8.3		12.2
53.20	1634			421.7	

radiation heat loss from power spikes to adjacent axial pellet gaps compensates for higher peak cladding temperatures on the power spikes.[21]

A series of tests[15] were conducted by EG&G Idaho, Inc., in the Power Burst Facility to determine an expected fuel behavior for the LOFT fuel bundles. Fabrication of these rods was similar to that for LOFT fuel rods, except that stable density fuel pellets were used for the LOFT lead rods.

The maximum amount of densification in the fuel rods used in the LOFT Lead Rod Tests is estimated to be less than 1%. Assuming the 1% maximum densification, the pellet volume change and, hence, the radial and length changes, are expected to be less than 33% that of the LOFT fuel pellets. The cladding temperature of the 1% densified fuel, compared with the as-received LOFT fuel in Figure 17, is only 10 K higher than that of the unstable LOFT fuel because of the smaller change in dimensions. Even if maximum densification were achieved in the LOFT Lead Rod Tests, the thermal behavior would be different than for fully densified LOFT fuel with no creepdown. Under these conditions, the cladding temperature in the LOFT Lead Rod Tests would increase only 10 K, compared with 106 K if LOFT fuel was used.

It is concluded from this study that (a) the stored energy is increased principally from increased power density due to the maximum changes in pellet dimensions and the corresponding changes in gap conductance and thermal conductivity and (b) the additional effect on stored energy from localized power spiking can be ignored because of the improved rod-to-rod heat transfer from radiation during a LOCE. There is evidence beyond the scope of this evaluation indicating that pellet cracking and relocation will nullify the effects of LOFT fuel densification on the cladding thermal response.

Formation of Axial Pellet Gaps

The radial and axial changes in pellet dimensions caused by fuel densification and pellet cracking, increase the potential to form axial pellet gaps during LOCEs which may result in (a) cladding waisting in fuel rods with axial pellet gaps and (b) localized power spikes in adjacent fuel rods.

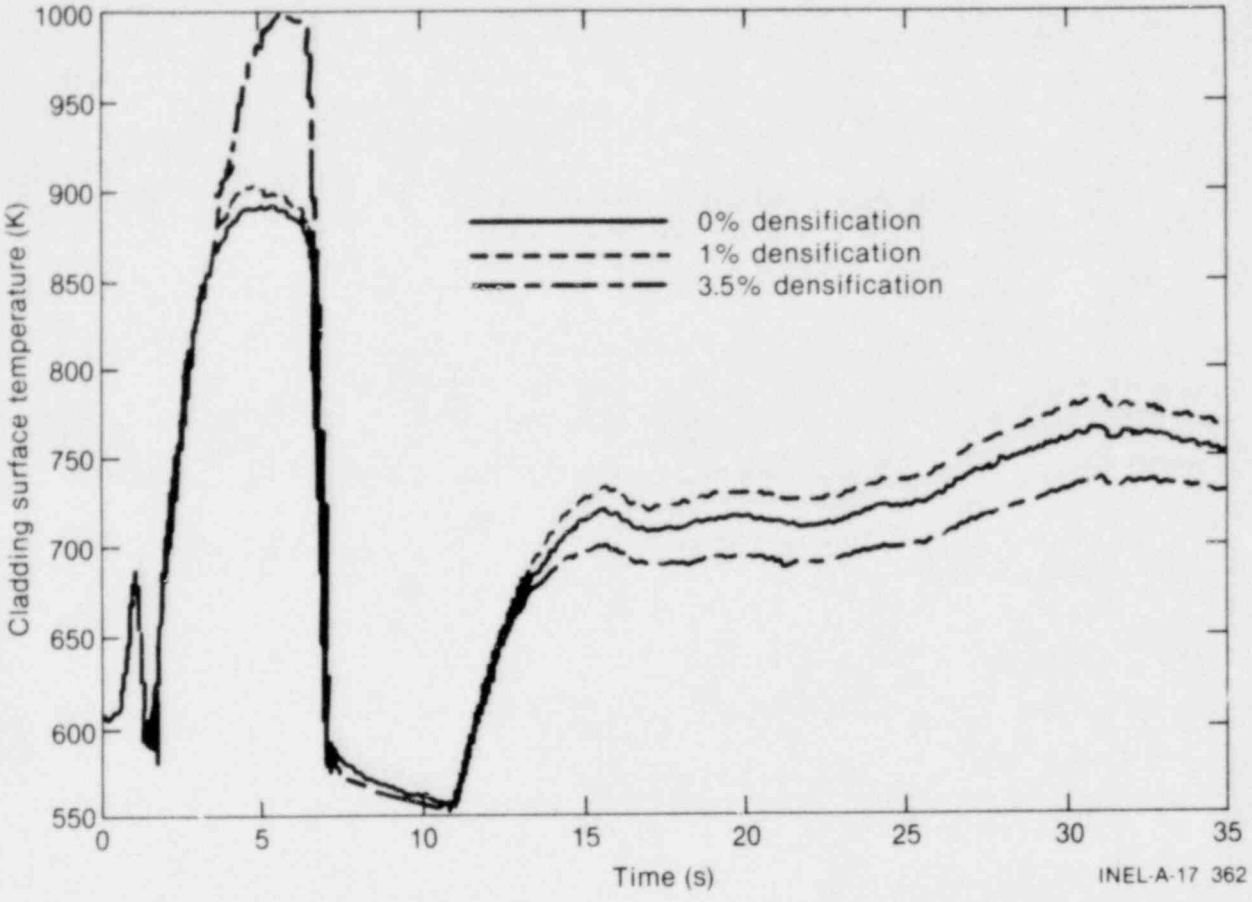

Figure 17. Cladding temperatures calcu ated using FRAP-T5 for fuel densified at 3.5, 1, and 0%.

Normally, at steady-state operating power levels, the axial pellet gaps at the axial hot plane are not greater than 0.25 to 0.38 mm due to differences in thermal expansion between the pellet center and the pellet surface. However, the increase in axial pellet gaps from densification cannot be determined with any degree of certainty. For the maximum decrease in pellet length caused by sintering, 1.34% for Lot 20-3 and 1.45% for Lot 20-5, the average maximum decrease of the 1.676-m UO_2 fuel stack length is 23.6 mm. Based on a final density of 96.5% TD, Exxon Nuclear Company[a] calculated maximum gap sizes varying from 40.6 mm for an initial value of 91.5% TD to 28.4 mm for an initial density of 93% TD.[22] These initial densities bracket the as-fabricated densities of Lots 20-3 and 20-5, but the Exxon results for both lots are higher than the 23.6-mm value derived from measured densification. The higher calculated values result from assuming that 1/2 of the volume change occurs in the axial direction.

Considering the small power levels near the ends of a fuel rod with a chopped cosine power profile, the fuel stack expands thermally only 17.8 mm at a 52-kW/m maximum linear power generation rate. If pellet hang-up occurs at full power near the midplane, an 8.9-mm axial gap would form at the center of the rod, since the bottom of the fuel stack would be free to drop down. Therefore, based on pellet hang-up occurring at the center of the fuel rod, the 8.9-mm gap from axial thermal expansion may be added to the 8.10-mm gap from fuel densification to result in a gap of 17.0 mm. Hellman et al.[21] studied the distribution of axial pellet gaps in full length PWR rods used in operating power reactors and determined a maximum possible gap of 35.6 mm occurring near the top of the fuel column and about a 25-mm gap

a. LOFT fuel manufacturer.

occurring near the center of a fuel rod. Taking into account the shorter fuel stack length in the LOFT 5.5-ft core than in commercial 12-ft cores, the maximum 17-mm gap expected for LOFT is consistent with the measurements of Hellman et al.[21]

The formation of axial pellet gaps may lead to cladding waisting (flow of cladding) into the axial gaps. Since waisting was observed[2] during elevated cladding temperatures of a LOCE in axial pellet gaps greater than 0.64 mm,[2] waisting can be a viable cladding deformation mechanism during the LOFT experiments. Axial gaps between 0.25 and 0.38 mm may form in the LOFT fuel rods from thermal expansion, and these gaps are expected to increase from densification. At present, axial pellet separation cannot be specified with certainty, but axial gaps greater than 0.64 mm are possible in the LOFT fuel.

In Figure 18, peak cladding temperatures for the hottest rod in the square peripheral module at 39.4 kW/m were combined with core pressures during a LOCE and superimposed on pressure-temperature curves representing zircaloy mechanical stability. Without fuel densification in these peripheral modules, the cladding is expected to remain freestanding. However, if maximum densification occurs, a 100-K increase in cladding temperature is expected at 39.4 kW/m; the zircaloy cladding is then expected to buckle. The temperatures shown in Figure 17 for the central

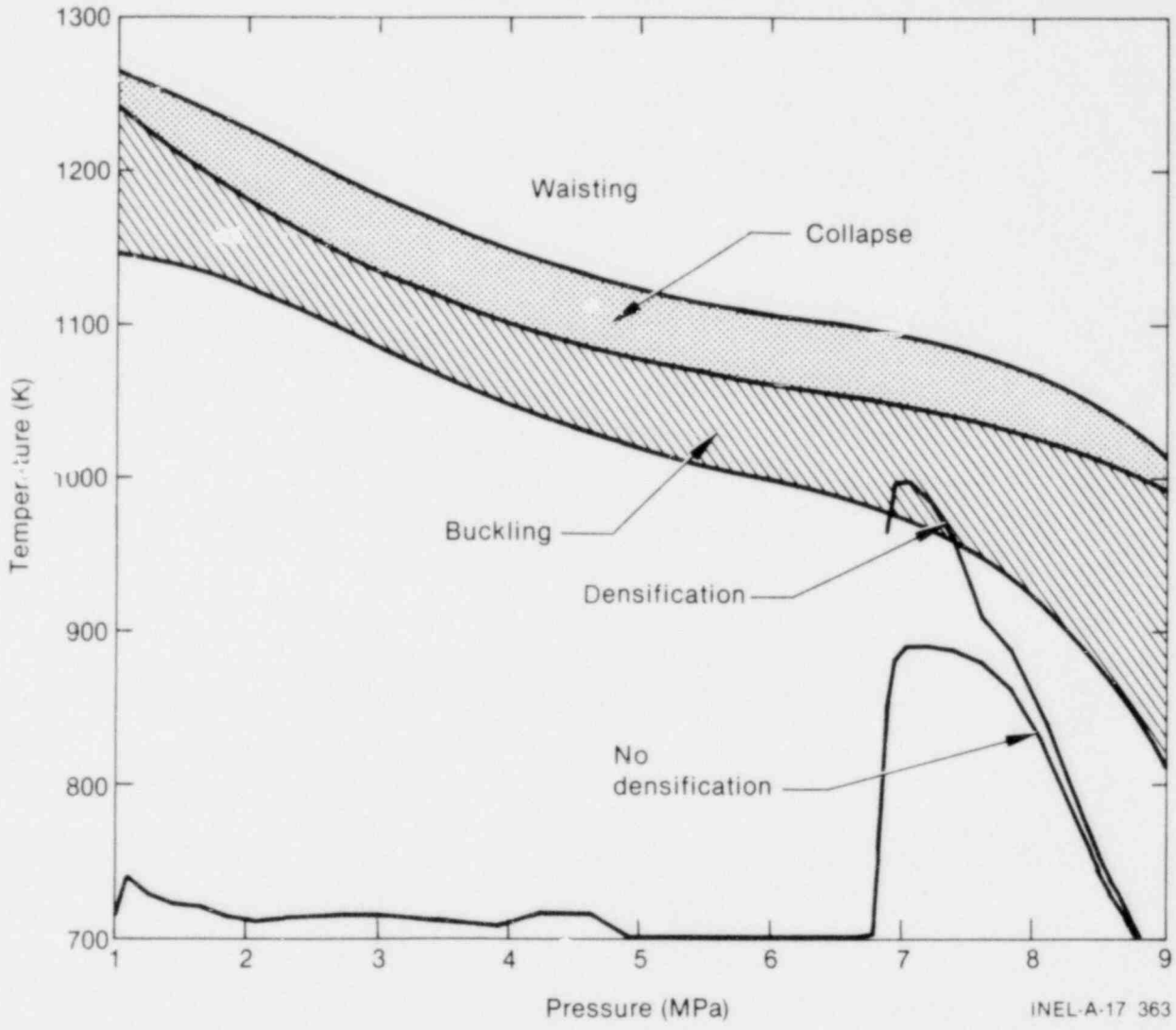

Figure 18. Effects of densification on the cladding mechanical stability for the square, peripheral fuel modules in LOFT.

module are not sufficiently high for cladding waisting, whether or not the fuel densifies.

The axial separation between pellets results in a localized power spike occurring in the fuel pellets in the vicinity of the gap, both on adjacent fuel rods and on the pellets bounding the gap. A 2.54-cm gap causes a 3.5% power spike on the nearest adjacent rods. This localized power spiking leads to increased fuel temperatures and correspondingly increased stored energy. Hellman et al.[21] showed that for the adjacent rod containing a gap, the temperature of the cladding near and over the gap is considerably lower than the cladding temperature that would occur with no gaps. Analysis of rod-to-rod heat transfer shows that the temperatures of the rods containing the gaps are sufficiently low to provide an effective radiation heat sink for the adjacent power-spiked rods.[21]

In conclusion, axial pellet gaps may form in the fuel stack from thermal expansion and densification. Although the distribution cannot be specified with any degree of certainty, axial gaps greater than 0.64 mm may form with the largest gap of about 17 mm.

CONCLUSIONS

The out-of-pile resintering tests on LOFT fuel pellets that were used to estimate in-pile densification showed that significant dimensional changes can occur in the fuel pellets after a 24-h resintering test; the densification for Lot 20-3 was 3.62%, with an accompanying 1.15% change in radius and a 1.34% change in length. Similar behavior was observed for Lot 20-5, with a 3.4% densification accompanying a 1.22% change in radius and a 1.51% change in length. The dimensional changes were anisotropic. However, the additional 10-h resinter from 14 to 24 h for Lot 20-5 resulted in a volume increase of about 0.25%. This swelling may be attributed to pore coalescence, with the pore pressure in equilibrium with the surface tension.

From the maximum changes in dimensions, from densification alone, the stored energy may be increased by 19% at 26.3 kW/m and 12% at 52 kW/m.

Densification is expected to be essentially complete by 1100 MWd/MtU, so that maximum densification is expected to occur during the design life of the fuel (2000 MWd/MtU).

For a power level of 39.4 kW/m, the cladding is not expected to waist or collapse uniformly around the pellets with either densified or undensified fuel. However, some buckling of the cladding may occur for the densified fuel if compensating effects of pellet cracking and relocation or cladding creepdown do not occur.

REFERENCES

1. A. F. J. Eckert, H. W. Wilson, K. E. Voon, *Program to Determine In-Reactor Performance of B & W Fuels - Cladding Creep Collapse*, BAW-10084, Rev. 1, November 1975.

2. C. S. Olsen, *Zircaloy Cladding Collapse Under Off-Normal Temperature and Pressure Conditions*, TREE-NUREG-1239, April 1978.

3. D. L. Reeder, *LOFT System and Test Description (5.5-ft Nuclear Core 1 LOCEs)*, NUREG/CR-0247, TREE-1208, July 1978.

4. D. A. Collins and R. Hargreaves, "Performance Limiting Phenomena in Irradiated UO_2," *Paper No. 50, BNES Nuclear Fuel Performance Conference, London, England, October 15-19, 1973.*

5. E. Rolstad, A. Hanevick, K. K. Knudsen, "Measurements of the Length Changes of UO_2 Fuel Pellets During Irradiation," *Enlarged HPG Meeting on Computer Control and Fuel Research, Halden, Norway, June 4-7, 1974.*

6. A. Hanevick et al., "In-Reactor Measurements of Fuel Stack Shortening," *Paper No. 89, BNES Nuclear Fuel Performance Conference, London, England, October 15-19, 1973.*

7. H. M. Ferrari, E. Roberts, J. Scott, "Fuel Densification Experience in Westinghouse Pressurized Water Reactors," *Paper No. 54, BNES Nuclear Fuel Performance Conference, London, England, October 15-19, 1973.*

8. T. J. Heal, J. E. Littlechild, R. H. Watson, "Development of Stable Density UO_2 Fuel," *Paper No. 52, BNES Nuclear Fuel Performance Conference, London, England, October 15-19, 1973.*

9. B. Burton and G. L. Reynolds, "The Sintering of Grain Boundary Cavities in Uranium Dioxide," *J. Nucl. Mat., 45*, 1972-73, pp. 10-14.

10. D. Hull and D. E. Rimmer, "The Growth of Grain-Boundary Voids Under Stress," *Phil. Mag.*, 4, 1959, p. 673.

11. M. O. Marlowe, "Predicting In-Reactor Densification Behaviour of UO_2," *Trans. ANS, 17*, November 1973, pp. 166-169.

12 *EEI/EPRI Fuel Densification Project*, EPRI 131, March 1975.

13. M. D. Freshly et al., "Irradiation-Induced Densification of UO_2 Pellet Fuel," *J. Nucl. Mat., 62*, 1976, pp. 138-166.

14. R. O. Meyer, *The Analysis of Fuel Densification*, NUREG-0085, July 1976.

15. D. J. Varacalle, Jr., et al., *PBF/LOFT Lead Rod Test Series Test Results Report*, NUREG/CR-1538, EGG-2047, July 1980.

16. C. S. Olsen, "UO_2 Pore Migration and Grain Growth Kinetics," *Paper C 1/9, 5th International Conference on Structural Mechanics in Reactor Technology, West Berlin, Germany, August 13-17, 1979.*

17. F. A. Nichols, "Theory of Grain Growth in Powers Compacts," *J. Appl. Phys., 37*, 13, December 1966, p. 4599.

18. D. L. Hagrman (ed.), *MATPRO - Version 11, A Handbook of Materials Properties for Use in the Analysis of Light Water Reactor Fuel Rod Behavior*, NUREG/CR-0497, TREE-1280, February 1978.

19. L. J. Siefken et al., *FRAP-T5 - A Computer Code for the Transient Analysis of Oxide Fuel Rods*, NUREG/CR-0840, TREE-1281, June 1979.

20 R. E. Williford et al., *The Analysis of Fuel Relocation for the NRC/PNL Halden Assemblies IFA-431, IFA-432, and IFA-513*, NUREG/CR-0588, PNL-2709, April 1980.

21. J. M. Hellman, C. A. Olson, J. W. Yang, "Thermal Behavior of Densification Power Spiked PWR Rods During a LOCA," *American Society of Mechanical Engineers, 75-HT-67*, April 1975.

22. S. F. Gains et al., *LOFT Fuel Densification Study*, XN-73-28, October 22, 1973.

APPENDIX A

LOFT UO_2 FUEL PELLET RESINTERING PROCEDURE

APPENDIX A

LOFT UO_2 FUEL PELLET RESINTERING PROCEDURE

This appendix outlines the procedure for resintering LOFT UO_2 fuel pellets out-of-pile through resintering tests to estimate the increase in pellet density during in-pile densification. Additionally, electron and optical metallography was performed on the pellets to determine the effect of resintering on pellet pore size and grain size. The resintering tests were performed on 4% enriched, unirradiated fuel pellets.

GENERAL PROCEDURE

The discussion in this section defines the general procedure followed for resintering, immersion density ,and void volume measurements, and electron and optical metallography of the fuel pellets during the resintering test. Pellet identification was maintained throughout the testing.

Resintering

A resintering cycle consisted of a heat soak (see Table A-1) at 1973 ± 15 K. The furnace atmosphere consisted of argon-6% hydrogen and was maintained at atmospheric pressure. The furnace temperature was not increased or decreased faster than 200 K/h. All pellets for each test were sintered at the same time. The hot zone of the furnace was such that all pellets in a heat were maintained at the prescribed temperature.

Pellet Density and Void Volume Measurements

Pellet density and void volume measurements were made as follows:

1. Pellets were baked out at 473 K for a minimum of 1 h. Argon flow was maintained at 34.5 to 69.0 kPa.

Table A-1. Pellet schedule for resintering, metallography, and void volume density measurements

	Number of Pellets					
	Resintered		Metallography		Void Volume Density	
Heat Cycle	Lot 20-3	Lot 20-5	Lot 20-3	Lot 20-5	Lot 20-3	Lot 20-5
As-received (total)	20	21	2	1	20	21
14 h at 1973 K	5	21	1	1	5	21
24 h at 1973 K	5[a]	20	1	1	5	20
14 h at 1973 K	5[b]		1		5	
24 h at 1973 K	5[a,b]		1		5	

a. Six pellets were taken from the 14-h resinter and resintered an additional 10 h for a total of 24 h.

b. Heat soaks were performed twice to verify data obtained from first sample lot.

2. Pellets were weighed at room temperature, and the dry weight (W_d) was recorded.

3. Pellets were placed in a small amount of H_2O containing one to two drops of photoflow wetting agent/100 mL H_2O. The pellets were evacuated for a minimum of 30 min using a vacuum dessicator and a liquid nitrogen cold trap in the vacuum line.

4. Pellets were removed from the water, and excess water was removed from the surfaces by rolling the pellets on a lint-free towel, saturated with water. The pellets were weighed, and the saturated weight (W_s) was recorded.

5. The immersion weight (W_I) of the pellets was determined by weighing pellets in a preweighed basket suspended in water. The immersion weight and water temperature and density (D_{H_2O}) were recorded.

6. The pellet immersion density, D_p, was calculated by

$$D_p = \frac{W_d}{W_s - W_I} \times D_{H_2O} \qquad \text{(A-1)}$$

where these terms are defined in Items 2, 4, and 5.

7. The pellet void, V_p, was calculated by

$$V_p = \frac{W_s - W_d}{D_{H_2O}} . \qquad \text{(A-2)}$$

Then,

$$V_p = \frac{W_s - W_d}{W_d} \times \frac{1}{D_{H_2O}} . \qquad \text{(A-3)}$$

Electron and Optical Metallography

One longitudinal and one transverse section of a fuel pellet were mounted and polished using a standard metallurgical procedure.

Electron Metallography. The specimen was vacuum coated with carbon using a standard metallurgical procedure. Each section was examined on the scanning electron microscope to determine size and distribution of pores less than 100 μm in diameter. Representative photomicrographs were taken of each section at the pellet center, midradius, and pellet periphery at suitable magnifications to adequately show the pore size and distribution. Four copies and a negative were obtained for each photograph.

Optical Metallography. The specimen was repolished to remove the carbon coating from electron metallography. The specimen was etched to reveal the grain boundaries in the fuel, and representative photomicrographs were taken to record the grain size at the pellet center, midradius, and periphery. Four copies and a negative were obtained for each photograph. The grain size was determined by the line-intercept method.

DETAILED PROCEDURE

Using information from the general procedure just described, the detailed procedure for performing the resintering tests is as follows:

1. Pellet immersion density and void volume on five as-received pellets were determined as per Table A-1 and the general procedure. These results were recorded.

2. Electron and optical metallography on two as-received pellets was performed as per Table A-1 and the general procedure.

3. One batch of pellets was resintered for 14 h ±15 min as per Table A-1 and the general procedure. Before resintering, the pellets were baked out as per the general procedure.

4. Void volume and immersion density measurements on five of the resintered pellets and metallography on the remaining pellet were performed as per the general procedure. These results were recorded.

5. One batch of four pellets was resintered for 24 h ±15 min as per Table A-1 and the general procedure. Before resintering,the pellets were baked out as per the general procedure.

6. Void volume and immersion density measurements and metallography on the five pellets were performed as per Item 4. These results were recorded.

7. The steps outlined in Items 3 through 6 were repeated to verify results.

APPENDIX B

TYPE C THERMOCOUPLE CALIBRATION DATA

APPENDIX B

TYPE C THERMOCOUPLE CALIBRATION DATA

The furnace and sample temperatures were measured during the resintering tests with a Type C, W-5% Re/W-26% Re, thermocouple. The calibration data for this thermocouple are listed in Table B-1.

Table B-1. Type C thermocouple calibration data[a]

Reference Junction Temperature = 32 °F
W5RE LOT Number 5258
W26RE LOT Number 26287

Temperature (°F)	Actual (MV)	Deviation (MV)[b]
200	1.282	-0.066
400	3.089	-0.076
600	5.072	-0.077
800	7.177	-0.063
1000	9.328	-0.062
1200	11.483	-0.078
1400	13.624	-0.099
1600	15.723	-0.128
1800	17.778	-0.152
2000	19.767	-0.180
2200	21.700	-0.196
2400	23.555	-0.217
2600	25.370	-0.204
2800	27.113	-0.188
3000	28.790	-0.163
3200	30.405	-0.125
3400	31.897	-0.131
3600	33.313	-0.129
3800	34.640	-0.123
4000	35.830	-0.148
4200	36.853	-0.213

a. Data provided by the vendor, the Claud S. Gordon Company, Richmond, Illinois 60071.

b. Deviation from IPTS 68 curve adopted 3-4-74.

APPENDIX C

PORE SIZE CHARACTERIZATION PROCEDURE

APPENDIX C

PORE SIZE CHARACTERIZATION PROCEDURE

This appendix outlines the procedure followed to determine the pore size and size distribution of pores in UO_2 fuel pellets during the resintering tests. The porosity characterization was performed on 4% enriched, unirradiated fuel pellets.

GENERAL PROCEDURE

The following discussion defines the procedure for obtaining the pore size and size distribution and corresponding total pore volume determinations.

Pore size and size distributions were obtained on longitudinal and transverse metallographic sections. On transverse sections, areas examined were at the pellet center, midradius, and edge. For longitudinal sections, areas measured were along the pellet axis at the pellet center, pellet end, and midway between the center and end of a pellet. The surfaces examined were polished, but unetched.

Pore Size

The pore size and size distribution were obtained with an Omnicon Alpha^{TM} Image Analyzer using the oversize or cumulative count. With this mode, the number of pores having a maximum horizontal chord larger than a predetermined size was determined. For pore sizes 1 μm and greater, pore sizes were determined directly from the Bausch and Lomb metallograph. For pore sizes less than 1 μm, pore sizes were determined from scanning electron microscopy (SEM) photographs obtained with at least 1000X magnification and with the Omnicon Alpha^{TM} Image Analyzer.

Pore Size Distribution

The pore size distribution was derived from the cumulative distribution by subtracting the pore count of successive size ranges, provided these readings were equidistant. If the size ranges were not equally spaced, the differences in pore count were multiplied by the relative spacing of the size range intervals to correctly shape the distribution. The pore size distribution was fitted to a normal distribution based on Equation (C-1):

$$y = \frac{V_p \, I}{s \sqrt{2\pi}} \exp\left(- \frac{(x - \bar{x})^2}{s^2} \right) \qquad \text{(C-1)}$$

where

y = ordinate of the distribution

I = pore size interval

s = standard deviation of the sample

x = pore size

$\bar{x}$ = average pore size

V_p = total pore volume.

Total Pore Volume

The total pore volume was calculated from the pore size determined from the cumulative distribution. Each pore was assumed to be spherical, and the total pore volume was calculated from the projected area of the spherical pores and the total area examined using Equation (C-2):

$$V_p = \frac{\sum_{i=1}^{N} \frac{\pi d_i^2}{4} N_i}{A} \qquad \text{(C-2)}$$

where

d_i = pore diameter (μm)

N_i = number of pores

A = total area examined (μm^2).

External Calibration

Before the pore size and size distribution were determined, the calibration factor for the image analyzer was verified. Although either a ruler with an accurate scale or the calibration slide with two patterns of circles of accurately known diameters can be used, calibration using area measurements was used since they produce the most accurate results. The area of the reference circle was measured with the image analyzer, and the displayed area was recorded. The calibration factor was calculated from Equation (C-3).

$$K = \frac{\text{actual area}}{\text{displayed area}} . \qquad \text{(C-3)}$$

Internal Calibration

The internal calibration of the image analyzer was also checked prior to making the pore size and distribution measurements, since the internal calibration was designed to maintain accurate relations among the various measurements. A circle on the calibration slide covered about 3/4 of the height of the field of measurement. The projected length and Feret's diameter were measured from the displayed value. These measurements were nearly identical. The area of the test circle was then measured from the display. The measured area agreed within 2% of the area calculated from $\pi L^2/4$ using one of the above measured lengths for L. If the values did not agree, the image analyzer was recalibrated.

DETAILED PROCEDURE

Using the general procedure just described, pore size and size distributions were determined as follows:

1. The pore size and size distribution on one longitudinal and one transverse section of the as-received pellets were determined. These results were recorded.

2. The pore size and size distribution on one transverse and one longitudinal section from each pellet resintered at 1973 K for 14 and 24 h were determined.